BACHELOR' S THESIS / BIOMEDICAL ENGINEERING 2024

Prediction of Seizure Onset Zone in epilepsy patients via a network coupling measure

Saioa Elizondo Urrutia

upf. Universitat Pompeu Fabra Barcelona

Prediction of Seizure Onset Zone in epilepsy patients via a network coupling measure

Saioa Elizondo Urrutia

Bachelor's thesis UPF 2023/2024

Thesis supervisor(s):

PhD Marc Grau Leguia, Department of Information and Communication Technologies
UPF

Universitat Pompeu Fabra Barcelona

Acknowledgments

I would like to express my most sincere gratitude to my supervisor, Marc Grau, for his invaluable suport, patience and insightful guidance throughout the realization of this thesis. Without his expertise and assistance, this work would not have been possible.

Additionally, I would also like to thank my family and friends for their constant suport and patience throughout this journey. Your encouragement has been a source of strength and motivation every day.

Summary/Abstract

Epilepsy, a chronic neurological disorder characterized by recurrent seizures, affects millions globally. For patients with drug-resistant epilepsy, surgical intervention becomes a viable option. However, precise localization of the seizure onset zone (SOZ) is crucial for successful surgery. This thesis investigates the potential of the L measure, a non-linear method analyzing directional couplings between brain regions, for SOZ detection in pharmacoresistant epilepsy patients using electroencephalography (EEG) data recorded in a natural environment.

We analyzed seizure dynamics in 10 patients using EEG data from the Melbourne NeuroVista Seizure Prediction Trial database. Applying the L measure, we explored connectivity patterns within and across brain regions during pre-ictal, seizure onset, and ictal stages. Network analysis using graph theory metrics assessed these variations across EEG channels and patients to identify potential SOZ locations. Furthermore, we developed a novel method, to track channel connectivity dynamics during seizures, potentially detecting the SOZ with higher temporal resolution.

These findings are expected to contribute to a more comprehensive understanding of seizure dynamics and the potential of the L measure for SOZ detection in pharmacoresistant epilepsy patients. This research may pave the way for improved surgical planning and treatment outcomes for this challenging patient population.

Keywords

Epilepsy, seizure, EEG, Seizure Onset Zone, L measure, directional coupling, network analysis, graph theory

Preface or prologue

Epilepsy, a chronic neurological disorder characterized by recurring seizures, disrupts the lives of millions of people worldwide. While the precise cause of epilepsy remains elusive, it often manifests as sudden bursts of electrical activity within the brain, leading to a variety of alterations in neural communication, from involuntary movements to changes in behaviour or awareness.

For many epilepsy patients, the most common treatment is medication. However, a significant portion of patients continue to experience seizures that are resistant to medication, posing a significant challenge for both patients and healthcare providers. Epilepsy surgery has emerged as a promising approach for these patients, aiming for the complete removal or disconnection of the epileptogenic zone (EZ), the area of the brain responsible for generating seizures. However, the success of this approach relies on precise localization of the seizure onset zone (SOZ), which is an area contained within the EZ and with an easier detection.

Recent advancements in epilepsy research have introduced new methods to improve the detection of SOZ. These include advanced techniques for analyzing EEG data, assessing functional connectivity between brain regions, and applying graph theory to study how the epileptic brain functions. One promising approach involves using nonlinear methods like the L measure to identify specific patterns in EEG signals, revealing complex relationships that contribute to seizure activity.

This thesis focuses on applying the L measure to EEG data collected from patients with pharmacoresistant epilepsy in everyday environments. By studying connectivity patterns and using graph theory metrics, our goal is to enhance our ability to pinpoint the SOZ accurately. This precision can significantly improve surgical outcomes, offering hope for better management of epilepsy.

Through a detailed analysis of data from the Melbourne NeuroVista Seizure Prediction Trial, we aim to uncover intricate network configurations that drive seizure dynamics. By understanding these complex interactions, our study contributes to a more comprehensive understanding of seizure dynamics. Ultimately, this knowledge could lead to the development of improved techniques for identifying and treating the SOZ, potentially transforming the lives of patients with drug-resistant epilepsy by offering more effective surgical options and improving their overall quality of life.

Index

List of Figures

List of Tables

1. INTRODUCTION

1.1 Epilepsy and resective surgery in pharmacoresistant patients

Epilepsy, a chronic neurological disorder characterized by recurring, unprovoked seizures, affects millions of individuals worldwide, posing significant challenges to both patients and healthcare providers [1]. Although the exact cause of epilepsy remains unknown, it is typically diagnosed when an individual experiences two unprovoked seizures or one unprovoked seizure with a high likelihood of recurrence. Not all seizures are caused by epilepsy; some may be attributed to factors such as brain injuries or familial predispositions [1].

Seizures, which are the main manifestation of epilepsy, result from sudden bursts of electrical activity within the brain, leading to alterations in neural communication. These abnormal electrical discharges can manifest in diverse forms, including involuntary changes in body movement, sensation, behaviour, or awareness [2].

Despite significant advances in epilepsy research and the development of antiepileptic drugs (AEDs) as the primary treatment modality, many epilepsy patients continue to experience recurrent seizures that do not respond to medication [3]. The International League Against Epilepsy (ILAE) defines drug-resistant epilepsy as the failure of adequate trials of two tolerated and appropriately chosen AED schedules to achieve sustained seizure freedom [5]. Drug-resistant epilepsy is particularly common in temporal lobe epilepsy (TLE) and significantly affects patients' quality of life. Moreover, AEDs can cause severe side effects, from toxicity to cognitive issues and depression, making managing refractory epilepsy even more challenging [4].

In recent years, epilepsy surgery has become a widely accepted option for managing medically refractory focal epilepsy in both adults and children [6]. The primary objective of this surgery is the complete removal or disconnection of the epileptogenic zone (EZ), defined as the area of cortex indispensable for the generation of clinical seizures. Doctors use a variety of diagnostic tools, including analysis of seizure behaviors, electrophysiological recordings, functional testing, and neuroimaging techniques, to define the location and boundaries of the EZ. These diagnostic methods delineate different cortical zones, including the seizure onset zone (SOZ), irritative zone, ictal onset zone, functional deficit zone, and the epileptogenic lesion, all of which provide clues about the EZ's location and size [7]. While the EZ cannot be measured directly, the localization of the SOZ, which is the area of the cortex from which clinical seizures are generated, provides indirect estimates of its location [9]. Moreover, the SOZ is commonly localized using scalp or invasive EEG techniques, such as intracranial electroencephalography (IEEG) [7].

However, not all resective surgeries completely stop seizures. Studies show that long-term seizure control is achieved in about 40-80% of eligible patients, with success rates higher in temporal lobe epilepsy (60-80%) compared to extratemporal lobe epilepsy (40-60%). For patients who continue to have seizures after surgery, managing their condition becomes more difficult and frustrating for both them and their doctors. Additional treatment options include adjusting antiepileptic drug (AED) regimens, using

interventions like vagus nerve stimulation (VNS) and responsive neurostimulation (RNS), or considering a second surgical procedure. While some of these approaches focus on managing symptoms, another surgery might offer a chance for achieving seizure freedom [10]. Taking that into account, both the efficacy of the initial resective surgery and any subsequent procedure would likely improve with more precise localization of the SOZ. Therefore, there is a pressing need to develop methods to better detect the SOZ.

1.2 State-of-the-art

There are a lot of different methods that have been used to try to detect SOZ. Recent advancements have introduced innovative approaches for localizing the SOZ in epilepsy patients. One study used EEG source imaging (ESI) and functional connectivity analysis to devise a non-invasive and objective technique, with potential applicability in clinical settings [8]. Another study proposed a pipeline combining spectral kurtosis-based channel selection and wavelet-based High-Frequency Oscillation (HFO) detection, demonstrating high sensitivity and specificity in identifying the HFO area overlapping with the clinically defined SOZ, while also significantly reducing computational time [10].

In recent years, researchers have also started to use brain connectivity and graph theory-based approaches to understand better the epileptic brain. They believe that the SOZ may show unique connectivity patterns, compared to other areas of the brain [11]. For example, Varotto et al. [12] studied drug-resistant epileptic patients and found distinct connectivity patterns in the EZ at the pre-ictal, ictal and inter-ictal periods.

For univariate methods, there are linear signal analysis methods which have been widely used to characterize the SOZ based on EEG recordings. Some of these are cross-correlation based analysis [13, 14] and frequency analysis based studies [15, 16]. However, linear methods lose important characteristics of seizure dynamics since they do not consider the directionality of the signals and the complex interactions between different regions for instance.

In contrast, non-linear methods offer a more sophisticated and accurate approach in trying to identify the SOZ. Non-linear techniques can detect nonlinearities and temporal dependencies in EEG signals that linear methods might miss. Moreover, they can handle better the irregular and complex nature of epileptic signals.

One of those methods is the nonlinear interdependence measure L. It was introduced by Chicharro et al. [17] and it is based on state space distances for detecting directional couplings in time series. This measure serves to characterize the interdependence between different brain areas involved in epileptic process. For instance, Grau et al. [18] used it in epilepsy patients' EEG signals and they successfully identified distinct connectivity structures across different seizure phases. The strongest connections were found in the SOZ, which confirms what is already known from epilepsy research. The average connectivity patterns over time showed how seizures start and stop, giving important clues about how connections change during seizures. Based on these studies, Moreno [19] conducted her Bachelor Thesis to test how well connectivity patterns identified by the L measure could be reproduced with new datasets. Her research also looked at how these patterns evolved during seizures. Furthermore, she used machine learning to classify electrodes as either focal or non-focal based on their connectivity profiles, with the goal of detecting the SOZ. However, questions remain regarding the broader applicability of

the L measure, and its application to data in a natural environment still needs to be explored.

1.3 Objective

The primary objective of this study is to analyze seizure dynamics in pharmacoresistant epilepsy patients in a natural environment and attempt to detect the SOZ. Specifically, we will analyze EEG seizure data from epilepsy patients recorded in natural settings, diverging from the typical clinical setting. Subsequently, we will apply the nonlinear L method to the selected EEG data to explore connectivity patterns before and during seizures, emphasizing inter-patient variability. Additionally, graph theory metrics will be employed to assess variations across EEG channels and patients, aiming to identify potential SOZ locations and network configurations. Finally, the influence received and gived by each EEG channel during the seizure evolution will also be analyzed to try to find potential SOZ sources.

2. METHODS

2.1 Data

2.1.1. Dataset characteristics

The data used in this study was obtained from the Melbourne NeuroVista Seizure Prediction Trial database [20]. The Melbourne NeuroVista trial was the pioneer trial of long-term EEG recordings conducted in an ambulatory setting for farmacoresistant focal epilepsy patients. It was a feasibility study to provide safety and proof-of-concept efficacy data for the seizure advisory system in patients with epilepsy. Patients were recruited between March 2010, and June 2011 and they were adults capable of managing daily activities independently who had a seizure frequency ranging from 2 to 12 seizures per month. The recruited patients received implantation of a seizure advisory system, comprising intracranial EEG recordings and an external advisory device. The system's components included silicon implantable lead assemblies with eight platinum iridium contacts each, which collected intracranial EEGs, and a telemetry unit that wirelessly transmitted data to the external device. The EEG system utilized 16 electrodes arranged into 4 electrode stripes, with each stripe containing 4 electrode channels.

In order to get access to the data a formal request had to be made to the Epilepsy Ecosystem platform [21] which serves as a collaborative platform aimed at enhancing the effectiveness of seizure prediction algorithms. Data from 12 out of the 15 patients who underwent the NeuroVista procedure are available there. Specifically, the data for patients 5, 12, and 14 are not included in the database. In the case of patient 5, complications arose in the data collection phase as the sutures of the implantable telemetry unit became compromised, leading to the migration of the device. For patient 12, seizure reporting showed a notorious deviation from the EEG recordings' pattern. Subsequent evaluation via inpatient video-EEG indicated that several events were psychogenic in nature [20].

Patient	Age (years)	Sex	Antiepileptic Drugs	Epileptogenic Zone	Previous Resection
Patient 1	26	Male	Yes	Parietal-temporal	No
Patient 3	22	Female	Yes	Parietal-temporal	Yes
Patient 6	62	Male	None	Temporal	No
Patient 7	52	Male	Yes	Frontotemporal	No
Patient 8	48	Male	Yes	Frontotemporal	Yes
Patient 9	51	Female	Yes	Occipitoparietal	No
Patient 10	50	Female	Yes	Frontotemporal	Yes
Patient 11	53	Female	Yes	Frontotemporal	No
Patient 13	50	Male	Yes	Temporal	Yes
Patient 15	36	Male	Yes	Temporal	Yes

Table 1. *Characteristics of the selected NeuroVista Seizure Prediction Trial patients at baseline. "Antiepileptic Drugs" denotes whether the patient was taking medications to manage epilepsy. "Epileptogenic Zone" indicates the region in the brain where seizures originate. "Previous Resection" indicates whether the patient had undergone surgical resection prior to the trial.*

As depicted in Table 1, out of the initial 15 patients, 10 were selected for this study. Patients 2 and 4 were excluded due to insufficient seizure data, which will be further explained in the subsequent section. Among the selected 10 patients, there were six men and four women, with ages ranging from 22 to 62 years (median age: 50 years). Among them, five patients had undergone prior epilepsy resection. Moreover, at study baseline, all participants except patient 6 were taking antiepileptic medications.

The database contains a folder for each patient and each one includes multiple .mat files, with each file representing a single seizure. Inside each file, there is a variable named 'data' with dimensions TxN, where T represents the data length and N represents the number of electrode channels (16). The length of T varies depending on the duration of the seizure. Seizure onset occurs at 1 minute and the sampling rate is 400Hz.

2.1.2. Data selection

Before proceeding with the analysis of the EEG dataset, it was crucial to conduct a comprehensive inspection. This initial step served several critical purposes: assessing data quality by identifying artifacts, noise, or irregularities; understanding the dataset's structure including channels, sampling rate, and recording duration; determining necessary preprocessing steps such as filtering and artifact removal; gaining insights into baseline characteristics of EEG signals like typical frequency ranges and amplitude variations; and uncovering potential trends or anomalies that could inform hypothesis generation and guide subsequent analysis strategies. This thorough inspection ensured that our analysis was based on reliable data, leading to robust and meaningful results.

Considering that Moreno [19] had already initiated the visual inspection of the Melbourne NeuroVista dataset, this study focused on reviewing the patients and seizures that remained pending examination. Additionally, other members of the UPF Nonlinear Time Series Analysis (NTSA) group contributed to this endeavour, as the task demanded considerable time and effort. As a result, the inspection workload was distributed among team members, with my responsibility being the examination of all seizures from patients 9 and 10, along with 18 seizures from patient 1. In total, I inspected a total of 573 seizures.

The inspection was carried out using a MATLAB [22] code. Each seizure recording was systematically examined using a 20-second moving window. The main artifact that was encountered was the dropout artifact which refers to a temporary loss or interruption of signal from one or more electrodes (Figure 1). This can occur due to technical issues such as poor electrode contact with the scalp, loose connections, or signal interference. Dropout artifacts can result in gaps or distortions in the EEG signal, potentially affecting the accuracy and reliability of the recorded data. Therefore, those recordings that contained any dropout artifact were discarded as the reliability of the L measure and subsequent measures would have been compromised. Besides dropouts, some recordings also presented an artifact that looks like a flat line. Unlike the dropout artifact which appears simultaneously in all the channels of the EEG, flat lines appear in single channels (Figure 2).

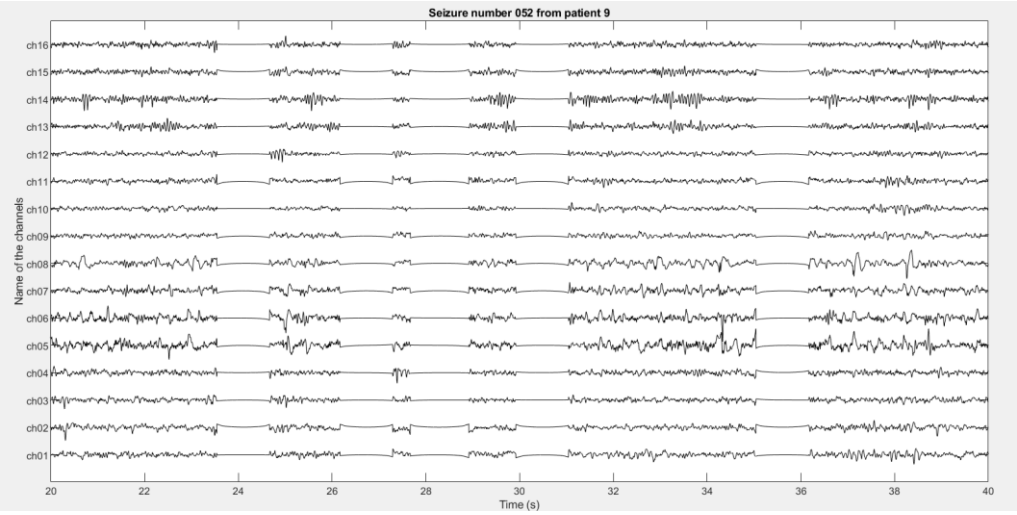

Figure 1. *Example of dropout artifacts in a seizure from patient 9. In the y axis each of the 16 EEG channels is displayed (Ch1,…,Ch16). The x axis represents the time. In the 20-second window shown five dropout occurrences are found in all sixteen channels at seconds 24, 26, 28, 30 and 36. These are characterized by sudden flatlines or abrupt changes in the signal amplitude, are evident across all channels.*

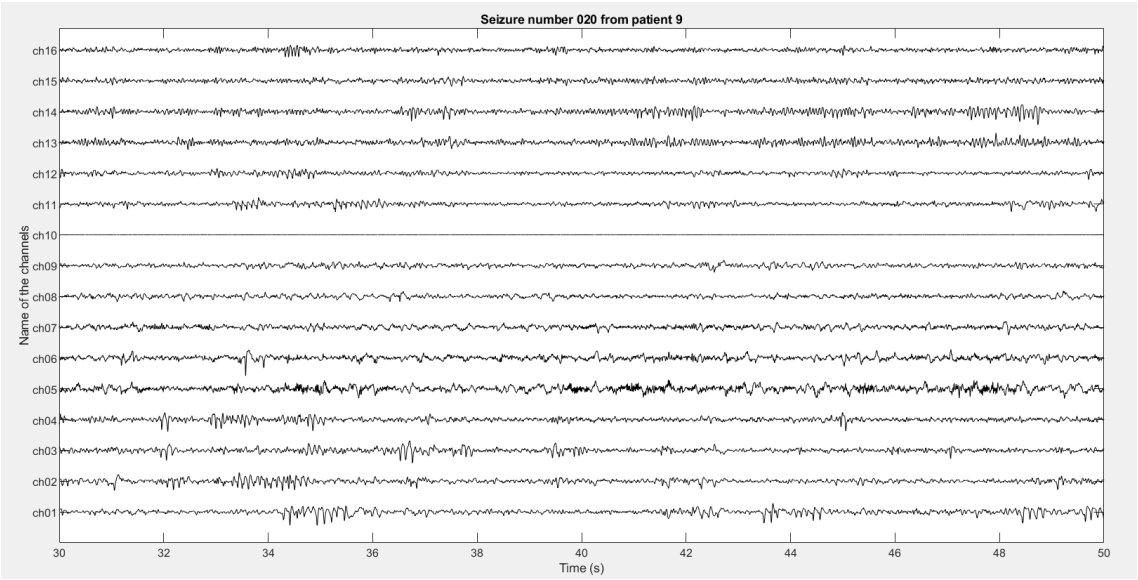

Figure 2. *Example of flat line artifact in a 20-second EEG window from patient 9. In the y axis each of the 16 EEG channels is displayed (Ch1,…,Ch16). The x axis represents the time. In this case the artifact affects only channel 10. This contrasts with the active seizure patterns observed in the other channels, indicating a localized issue with the recording in this channel.*

As previously outlined, from the initial 12 patients that were made available by the NeuroVista team, 10 were ultimately selected. During the data selection stage, it was observed that patients 2 and 4 contained very few artifact-free seizures, specifically, 10 and 6, respectively. Given the limited amount of usable data, it was determined that including these patients would compromise the generalizability of the results. Consequently, these patients were excluded from the study.

2.2 L measure

In this study, the L measure is employed to analyse multichannel EEG recordings to identify directional coupling between different brain regions during seizures. As noted earlier, the L measure was introduced by Chicharro et al. [17]. It is derived from the asymmetric state similarity criterion and serves as a detector of directional couplings between two dynamical systems. For instance, suppose we have two dynamical systems, X and Y, from which we extract scalar signals x_i and y_i for $i = 1, \ldots, N$. These signals are used to reconstruct the state space of the dynamics using delay vectors, where m is the embedding dimension and τ is the time delay. So, the index i now ranges from $i_0 = 1, \ldots, N = 1, \ldots (m-1)\tau$, that way the delay vector with index i has the scalar value with the same index i as a leading element. Next, the k spatially nearest neighbours of x_i and y_i are computed using the Euclidean distance. Temporally nearest neighbours are discarded using a Theiler window of length T. Then, the distances between of x_i and $x_{i\neq 0}$ are sorted, and g_{i,i_0} is introduced, which represents the rank of distances between x_i and x_{i_0} in an ascending list. Finally, to quantify the interdependence from X to Y, we define L(X|Y). For that, taking the X dynamics as reference, we define the Y-conditioned mean rank as $G_i^k(X|Y) = \frac{1}{k}\sum_{j=1}^{k} g_{i,w_{i,j}}$. Moreover, we define $G_i^k(X) = \frac{k+1}{2}$ and $G_i(X) = \frac{N}{2}$ as the mean and minimal mean rank respectively. With that, the L(X|Y) is defined as:

$$L(X|Y) = \frac{1}{N}\sum_{i=1}^{N} \frac{G_i(X) - G_i^k(X|Y)}{G_i(X) - G_i^k(X)}$$

For the case of L(Y|X) the roles of X and Y will have to be exchanged. Then, for identically synchronized dynamics (that is, X = Y), L(X|Y) = 1. In contrast, for independent dynamics, the expected value of L(X|Y) will be distributed around zero.

The values for the parameters of the L measure are the ones used in [18, 19]. We set the number of nearest neighbours to k = 5, the embedding dimension m = 5, the time delay τ = 5 and the Theiler window T = 15.

2.2.1 Application of L measure to multichannel EEG

The above-mentioned L measure was defined as a bivariate measure. However, the EEG data used in this work is a multichannel EEG recording. Therefore, in order to measure the directional coupling in the selected dataset each pair-wise combination for all the 16 EEG channels had to be considered. Then, instead of a single L measure, a 16x16 L matrix was obtained.

Given the vast amount of seizure recordings in the dataset, the High-Performance Computing (HPC) resources at UPF were used to solve the L measure computations efficiently and rapidly. In accordance with that, the EEG recordings were also downsampled by a factor of 2 to accelerate computations. Furthermore, as the focal point of interest was observing variations in the L measure throughout the EEG recording duration, calculations were performed using a moving window approach with 87.5% overlap. This involved analyzing data in 8-second intervals with a 7-second overlap between consecutive windows.

2.3 Network Analysis

Graph theory metrics were chosen to analyse the network structure of EEG seizures due to their ability to provide a detailed and comprehensive understanding of the complex interactions within the brain [23]. Graph theory models the brain as a network where nodes represent EEG electrodes and edges represent the connectivity between them, offering a powerful framework to study the intricate relationships and dynamics that occur during seizures [24]. In this study, the L measure matrix was employed to construct the graphs due to its robust ability to capture the directional coupling between EEG channels. By transforming the multichannel EEG data into a 16x16 L matrix, it becomes possible to analyze the directional dependencies between each pair of EEG electrodes, offering a detailed mapping of how different brain regions interact over time. Notably, to retain all relevant information, no thresholding was applied, yielding weighted graphs. Previous studies have demonstrated that performing an EEG graph theory analysis while preserving the weights from the connectivity matrices after the proportional thresholding step leads to more consistent results across network densities [25]. Moreover, given the asymmetry of the L matrix, the resultant graphs were directed. Consequently, our analysis focused on metrics tailored for weighted and directed networks, including shortest path length, clustering coefficient, betweenness centrality, and node strength. These metrics were computed using the Brain Connectivity Toolbox in Matlab [26].

Each metric was systematically applied to analyze selected seizures from our patient cohort. To facilitate comprehensive analysis, each seizure was segmented into three distinct periods. The pre-seizure period covered the initial portion of the recording up to 60 seconds before the seizure onset. The seizure onset period included windows starting from the onset marker up to the second 60 seconds, representing the initiation phase of the seizure. Subsequently, the seizure activity period encompassed the remaining windows capturing ongoing seizure activity. This division allowed us to assess metric variations across different phases of seizure progression. Additionally, computing average metric values facilitated the examination of inter-patient variability, providing insights into how seizure dynamics manifest uniquely across individuals. This structured approach enhances our understanding of epileptic network dynamics and might aid in identifying the SOZ.

2.3.1 Shortest path

The shortest path problem in graph theory, aims to identify the path between two nodes in a graph that minimizes the cumulative weight of its constituent edges [27]. In this work, Dijkstra's algorithm is used to obtain the shortest paths and it calculates the shortest path from a source node s to all other nodes v [28]. It updates the distance estimates d(v) iteratively, selecting the nodes based on the smallest d(u) from the set of unvisited nodes. The algorithm then adjusts d(v) for each neighbour v of u if a shorter path through u is discovered, determined by the edge weight w(u,v). The update step is:

$$d(v) = \min\left(d(v), d(u) + w(u, v)\right)$$

This process continues until all nodes are visited. Upon termination, the distance estimate of each visited node represents the shortest path from the source node [29].

In this study, we store the average number of edges in the shortest paths of each node. This metric directly reflects the network's interconnectedness and the efficiency of information exchange between brain regions. Fewer edges in these paths indicate more direct and efficient information transfer, whereas more edges suggest less direct or efficient flow of information between regions.

During seizure onset, an increase in the average number of edges could indicate heightened network activity and potential reorganization as the brain transitions into a seizure state. In the EEG context, this suggests that electrode channels in the SOZ might exhibit a higher number of edges at seizure onset.

2.3.2 Clustering coefficient

The clustering coefficient is a key measure in network theory, quantifying the degree to which nodes in a graph form tightly knit groups, providing insights into local connectivity patterns. For a node v with k_v neighbours, the clustering coefficient C_v is the ratio of the actual number of edges between neighbours to the possible number of edges, given by:

$$C_v = \frac{2t_i}{k_i(k_i-1)}$$

where t_i is the number of triangles around node i. The overall clustering coefficient C is the average of C_v across all nodes [23].

This measure helps to understand the local connectivity and modular organisation of brain networks during seizures. In EEG studies, a high clustering coefficient indicates that brain regions tend to form densely interconnected clusters, reflecting functional segregation [30]. Thus, in the context of this study, a high clustering is expected for the channels in the SOZ because the dense clustering could facilitate the rapid synchronization of neuronal activity.

2.3.3 Betweenness centrality

Betweenness centrality identifies critical nodes that act as bridges within the network, influencing information flow [31, 32]. It is defined as the fraction of all shortest paths in the network that pass through a given node v:

$$BC(v) = \sum_{h \neq j \neq v} \frac{\rho_{hj}(v)}{\rho_{hj}}$$

where ρ_{hj} is the number of shortest paths between h and j, and $\rho_{hj}(v)$ is the number of shortest paths between h and j that pass through v [23].

In EEG connectivity analysis for seizure data, betweenness centrality identifies critical nodes that influence seizure dynamics. High betweenness centrality nodes are vital for maintaining communication across the network [23]. During seizures, these nodes often have high centrality pre-ictally, especially near the seizure onset zone (SOZ), indicating their role in early seizure propagation. Their prominence typically decreases during the seizure but may increase again post-ictally [33]. In this work, betweenness centrality will be computed to try to find the channels that might be involved in the SOZ.

2.3.4 Node strength

Node strength is a measure of the cumulative weight of all connections a node has with its neighbours, capturing the node's activity level and centrality. For a node i, the node strength S_i is calculated as:

$$S_i = \sum_{j \in N(i)} w_{ij}$$

Where *N(i)* is the set of neighbours of node *i*, and w_{ij} is the weight of the connection between nodes *i* and *j* [23].

Higher node strength values suggest that these nodes are central hubs in the network, highlighting their importance in brain connectivity [34]. For this study, higher node strength might indicate regions with dense connectivity, potentially corresponding to the SOZ. Moreover, an increase in node strength pre-ictally may signal an impending seizure, while post-ictal decreases might reflect a stabilization or recovery phase of the network.

2.3.5 Statistical Analysis

To determine the statistical differences between seizure periods, we first calculated the differences between pre-seizure, seizure onset, and post-seizure data. We performed the Lilliefors test for normality on the differences [35]. Based on the results, if the data were normally distributed, a paired t-test was applied [36]; otherwise, the non-parametric Wilcoxon signed-rank test was used [37]. Specifically, we compared pre-seizure to seizure onset, pre-seizure to post-seizure, and seizure onset to post-seizure periods, applying the appropriate statistical test for each pair based on normality results.

2.4 Channel Influence Evolution

Building on the findings by Grau et al. [18], which highlight high overall connectivity during seizures with an initial directional bias from the SOZ to other brain regions, this study aimed to develop a method for SOZ identification using EEG channel data. For every time window within a seizure, the net impact $N_i(t)$ of each channel was determined using the L matrix values, which capture the difference between outgoing and incoming connections for each channel:

$$N_i(t) = O_i(t) - I_i(t) = \sum_{j \neq i} L_{ij}(t) - \sum_{j \neq i} L_{ji}(t)$$

Here, $O_i(t)$ represents the sum of weights of connections from channel i to all other channels within time window t, and $I_i(t)$ represents the sum of weights of connections to channel i from all other channels within the same time window t.

This approach tracks how channel influence changes over time, aiming to detect channels that exhibit significant connectivity alterations early in seizures, critical for SOZ identification. The method systematically evaluates each channel's net influence across pre-seizure and seizure periods, leveraging data aggregation across multiple seizures per patient to detect consistent connectivity patterns. Channels consistently showing significant alterations serve as robust indicators of the SOZ, enhancing accuracy in SOZ localization.

3. RESULTS

3.1. Data selection

As shown in Table 2, we analysed data of 10 out of the 15 available patients. On average, each patient contains 295 seizures, with a range from 71 to 484 seizures per patient. This results in a combined total of 3,409 seizures. Out of these, 1,397 seizures were free from artifacts. The average length of seizures varies significantly among patients, with values ranging from 29 seconds to 131 seconds. The overall average seizure length across all patients is 58 seconds. The duration of seizures also exhibits a wide range, with the shortest recorded seizure lasting 12 seconds and the longest extending to 560 seconds. The variability in seizure duration and the presence of artifacts underscore the importance of meticulous data handling to ensure the reliability and validity of the study's findings.

Patient	Total seizures	Artifact free seizures	Average seizure length (seconds)	Seizure duration range (seconds)
1	121	60	44	28 – 110
3	341	249	29	17 - 104
6	71	63	131	65 - 302
7	246	175	38	27 -105
8	466	40	49	24 - 132
9	204	87	70	42 - 145
10	484	284	51	12 - 560
11	463	18	32	19 - 76
13	481	356	36	21 - 78
15	77	50	67	54 - 84
Total	**3.409**	1.397	58	

Table 2. *Summary of the analyzed patient recordings. The "Total seizures" column indicates the total number of seizures recorded per patient during the study period. The "Artifact-free seizures" column specifies the number of seizures that were identified as artifact-free and suitable for analysis. The "Average seizure length (seconds)" column displays the average duration of seizures across all patients, illustrating the variability in seizure duration observed in the dataset.*

3.2. L measure applied to EEG

Table 2 indicates that each of the ten analysed patients exhibits a distinct seizure length. Visual inspection revealed differences observed in the frequency of spikes and the amplitude of seizure activities across these patients. To illustrate these differences, we selected a mild seizure (Figure 3) from Patient 7 and a more intense seizure (Figure 4) from Patient 6, based on variations in seizure length and amplitude. These figures provide detailed analyses of seizures captured through multichannel EEG recordings and corresponding L-value matrices at different time windows, showcasing diverse seizure patterns.

In Figure 3, the seizure is characterized as small and of low connectivity. The top panel displays the EEG recording over approximately 90 seconds. The seizure activity becomes notable around the 60-second mark (seizure onset stage) but remains relatively mild compared to the second seizure. This lower intensity is reflected in the L value matrices at different time windows. At time window 25, the EEG shows stable activity with low amplitude, and the L matrix indicates minimal connectivity with a few isolated regions of higher values, suggesting limited interaction between channels. At time window 60, at seizure onset, the EEG shows more pronounced spikes but still relatively low-intensity activity. The L matrix reveals increased connectivity values, indicating some level of synchronization between brain regions. During the seizure at time window 80, the EEG shows moderate high-amplitude discharges, and the L matrix presents a more complex connectivity pattern, but the values remain lower than those in the second seizure, reflecting less extensive neural interactions.

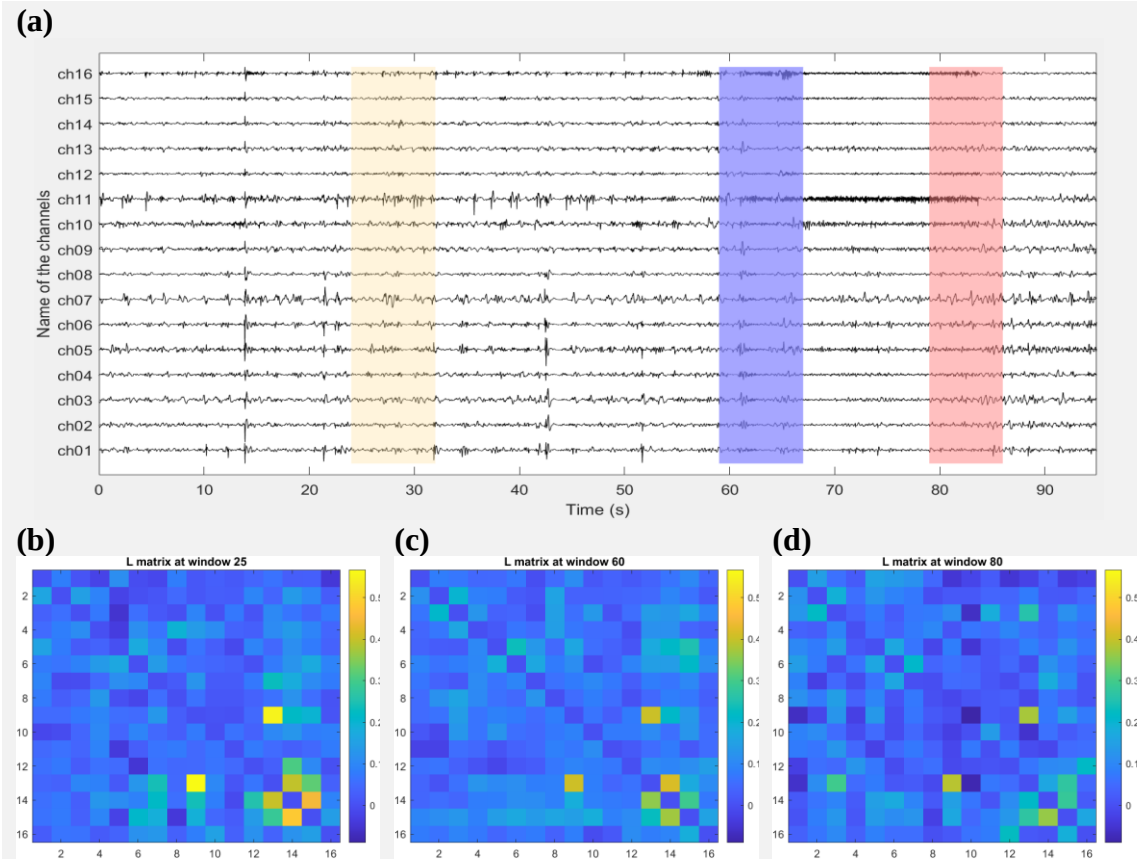

Figure 3. *Example of a small and low-connectivity seizure from patient 7. (a) The multichannel EEG recording of the entire seizure, with seizure onset at the 60th second. The bottom panel displays matrices with channel pair-wise L values at three different time windows of the seizure. (b) L matrix during the pre-seizure phase, covering the time window from 24 to 32 seconds (highlighted in yellow on the EEG). (c) L matrix at seizure onset, covering the time window from 59 to 67 seconds (highlighted in purple on the EEG). (d) L matrix during the seizure, covering the time window from 79 to 86 seconds (highlighted in red on the EEG).*

In figure 4, the seizure is significantly longer, has higher amplitude and exhibits higher connectivity. The top panel depicts the EEG over approximately 230 seconds. Seizure activity starts around the 60-second mark and peaks between 90 and 200 seconds, with intense, high-amplitude, and synchronized discharges. Additionally, channels 9 to 16

exhibit higher amplitudes compared to channels 1 to 8. This activity is mirrored in the L value matrices. At time window 25, similar to the previous seizure, the early-stage EEG shows stable, low-amplitude activity, and the L matrix indicates low connectivity values, consistent with a pre-seizure state. As the seizure onset approaches, at time window 60, the EEG begins to show more pronounced activity, and the L matrix shows increased connectivity values, indicating the beginning of synchronization between channels. At the peak of the seizure, at time window 160, the EEG shows intense, high-amplitude discharges across multiple channels, and the L matrix reveals significantly higher connectivity values, indicating extensive neural synchronization.

These differences highlight the varying nature of seizures, with the first example representing a milder event with lower connectivity, and the second example depicting a more severe seizure with more connectivity between channels. The L value matrices effectively capture these differences, providing a quantitative measure of the connectivity changes corresponding to the varying intensities of the seizures observed in the EEG recordings.

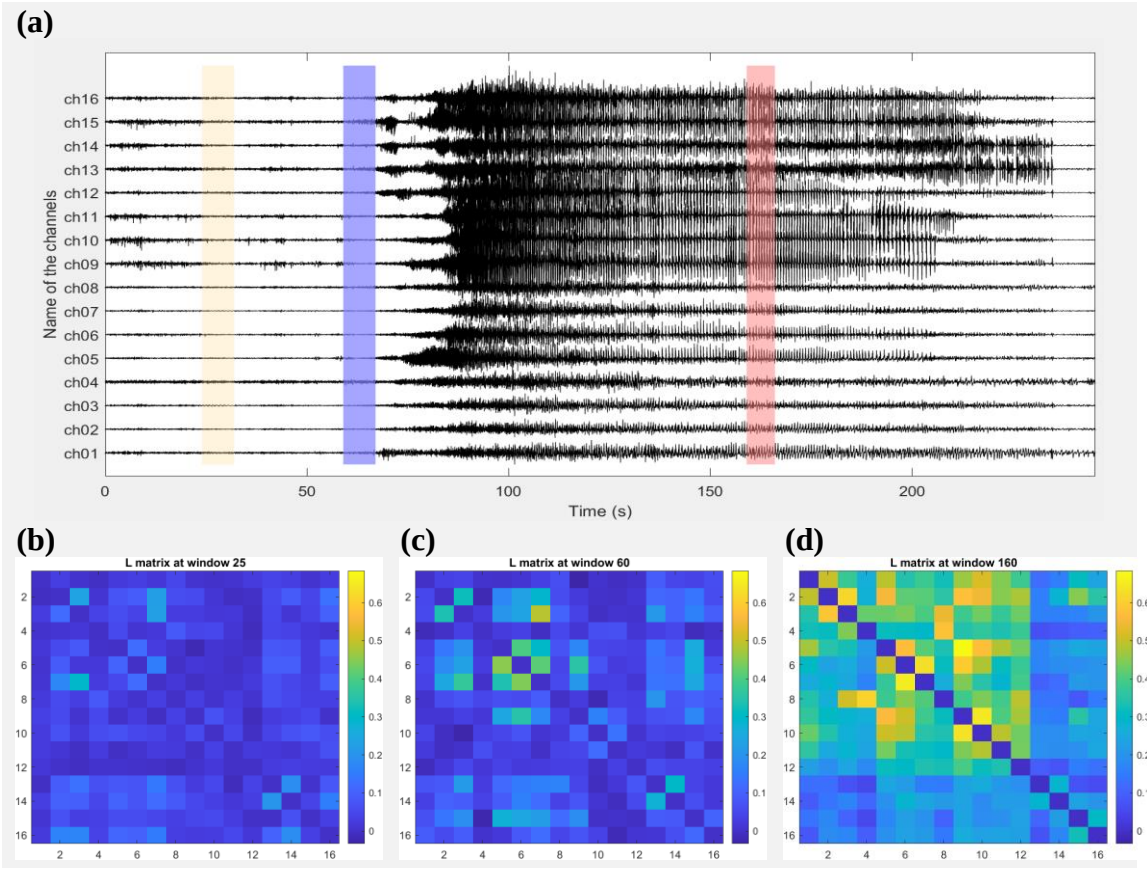

Figure 4. *Example of a big and high-connectivity seizure from patient 6. (a) The multichannel EEG recording of the entire seizure, with seizure onset at the 60th second. The bottom panel displays matrices with channel pair-wise L values at three different time windows of the seizure. (b) L matrix during the pre-seizure phase, covering the time window from 24 to 32 seconds (highlighted in yellow on the EEG). (c) L matrix at seizure onset, covering the time window from 59 to 67 seconds (highlighted in purple on the EEG). (d) L matrix during the seizure, covering the time window from 159 to 167 seconds (highlighted in red on the EEG).*

To further analyze the differences in connectivity profiles among patients, the relationship between the mean connectivity across all channels during seizures (from second 60 onwards) and the seizure length was studied (Figure 5). The figure illustrates a broad spectrum of seizure lengths and mean connectivity values across the patient cohort. For instance, Patient 13, who had the highest number of analyzed seizures (refer to Table 2), consistently shows low connectivity (between 0.05 and 0.15) with shorter seizures. In contrast, Patient 15 exhibits the highest average mean connectivity (ranging from 0.2 to 0.3) and slightly longer seizures compared to the majority. Patient 7, 8 and 11 generally demonstrate low connectivity, except for some outliers that display higher average connectivity. Conversely, Patient 6 presents seizures spanning a broader range of lengths with higher mean connectivity, indicating more extensive neural synchronization during their seizures. Patient 9 has a similar pattern as Patient 6, but its seizures are a little bit shorter. Overall, the scatter plot underscores significant variability in seizure characteristics among the patients, revealing diverse seizure patterns and neural dynamics.

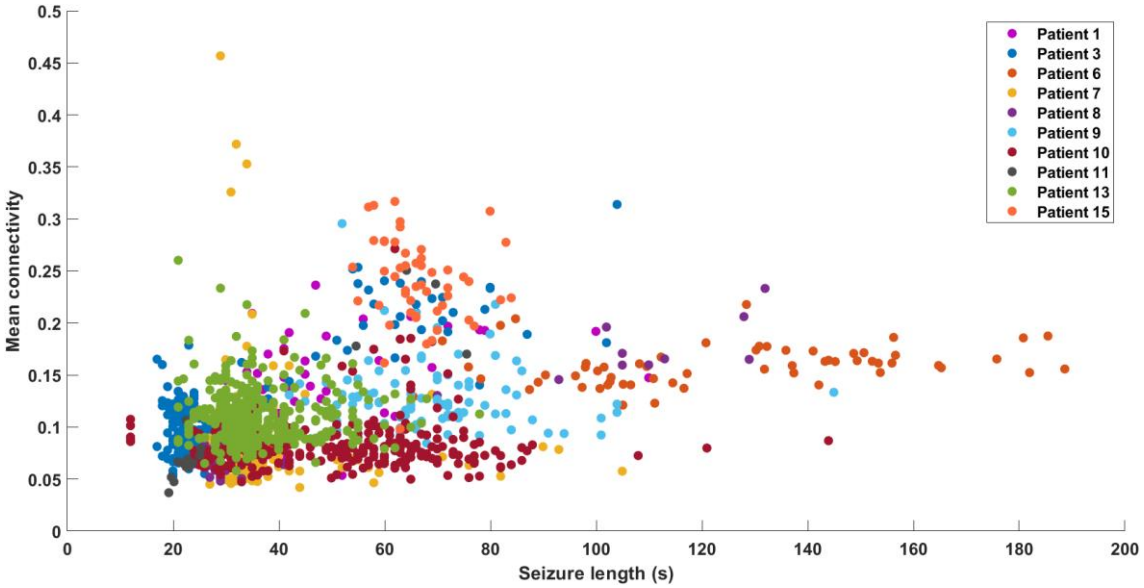

Figure 5. *The figure displays a scatter plot illustrating the relationship between seizure length (in seconds) and mean connectivity for different patients. Each dot represents a seizure event, color-coded by patient.*

To better illustrate these findings from the scatter plot, we computed the average connectivity profiles across all seizure time frames for all patients. In Figure 6.a, the average connectivity profile for Patient 7 reveals consistently low connectivity levels both before and during seizures. There's a slight increase at seizure onset, although this rise is relatively modest in absolute terms. Figure 6.b displays the average connectivity profile corresponding to the seizure depicted in Figure 3. Here, the connectivity pattern aligns closely with the patient's overall average, maintaining stability throughout the recording period as shown in Figure 3.

Patient 6 presents a different scenario. As shown in Figure 7.a, the mean connectivity starts from a lower baseline and remains relatively stable until approaching seizure onset, where a noticeable increase occurs. This elevation continues until approximately the 80th window, indicating heightened connectivity during this period. Subsequently, connectivity fluctuates but generally declines, with another significant peak observed

around the 150th window before tapering off. For the specific seizure depicted in Figure 7.b, similar to the average profile, connectivity begins low, increases sharply at seizure onset, and exhibits significant fluctuations throughout. Notably, this seizure displays a prominent peak after the 150th window, surpassing the peak observed in the average profile. At times, the seizure's connectivity exceeds the average plus standard deviation, highlighting moments of exceptionally high connectivity during certain seizures.

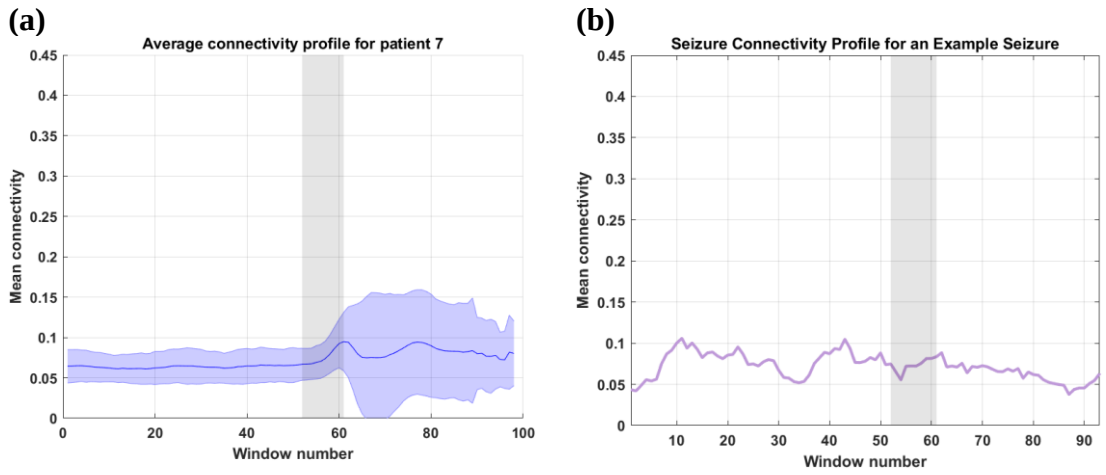

Figure 6. *The figure illustrates the connectivity profiles for seizures from patient 7. Panel (a) displays the average connectivity profile across all seizures for this patient, with the shaded area representing the standard deviation. The x-axis denotes the window number, while the y-axis represents the mean connectivity. Panel (b) presents the connectivity profile for a single seizure from patient 7, which corresponds to the seizure shown in Figure 3. In both (a) and (b), the seizure onset is shaded in grey.*

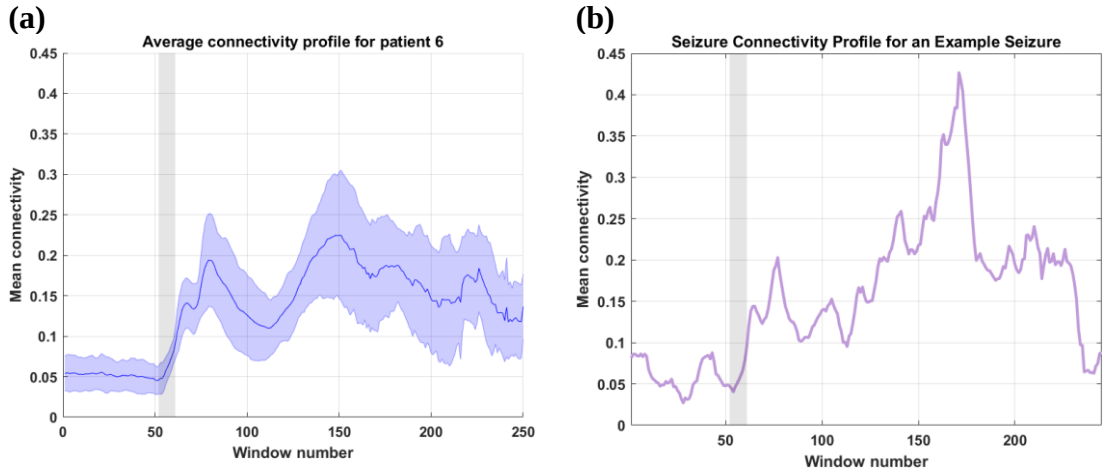

Figure 7. *The figure illustrates the connectivity profiles for seizures from patient 6. Panel (a) displays the average connectivity profile across all seizures for this patient, with the shaded area representing the standard deviation. The x-axis denotes the window number, while the y-axis represents the mean connectivity. Panel (b) presents the connectivity profile for a single seizure from patient 6, which corresponds to the seizure shown in Figure 4. In both (a) and (b), the seizure onset is shaded in grey.*

In general, as observed in the EEG recordings in previous sections and depicted in the scatter plot in Figure 5, comparing the connectivity profiles of Patient 6 and Patient 7 reveals distinct patterns during seizure activity. While both patients exhibit increased connectivity at seizure onset, Patient 6 demonstrates more pronounced and variable peaks in connectivity throughout the seizure compared to the generally low and consistent connectivity observed in Patient 7. These differences highlight unique neural dynamics and seizure characteristics between the two patients.

For the rest of the patients (Figure SI-1), the connectivity profile during the seizure closely resembles the mean connectivity patterns depicted in Figure 5. As noted earlier, Patients 1, 9 and 15 reach higher connectivity values throughout the seizure, whereas the rest of the Patients stay at low levels, close to the baseline connectivity. Moreover, in all of them there is a slight or moderate increase in connectivity around the window 60, corresponding to the seizure onset.

3.3. Network Analysis

3.3.1. Example patient network

Building upon the observations from Section 3.2, which explored individual seizure characteristics through visual inspection of EEG recordings and L value matrices, Section 3.3.1 delves deeper into the analysis by applying network analysis techniques. Here, we will focus on a specific patient (Patient 9) to illustrate how the L measure data is used to construct brain networks and how various network metrics reveal changes in network structure during different seizure phases (pre-seizure, seizure onset, and post-seizure).

For instance, the analysis of the average shortest path across the 16 EEG channels during pre-seizure, seizure onset, and post-seizure phases reveals significant changes in the brain's network structure (Figure 8). In the pre-seizure phase, the average path lengths are moderate, indicating that information transfer is quite direct and efficient. At seizure onset, the average path lengths increase notoriously in all channels, suggesting the network becomes more decentralized and less cohesive. During the seizure phase, following seizure onset, there is a dramatic decrease in the shortest path, indicating a highly centralized network structure with nodes being more directly connected. Moreover, it is important to note that all channels exhibit similar patterns, making the identification of the SOZ challenging with this measure alone

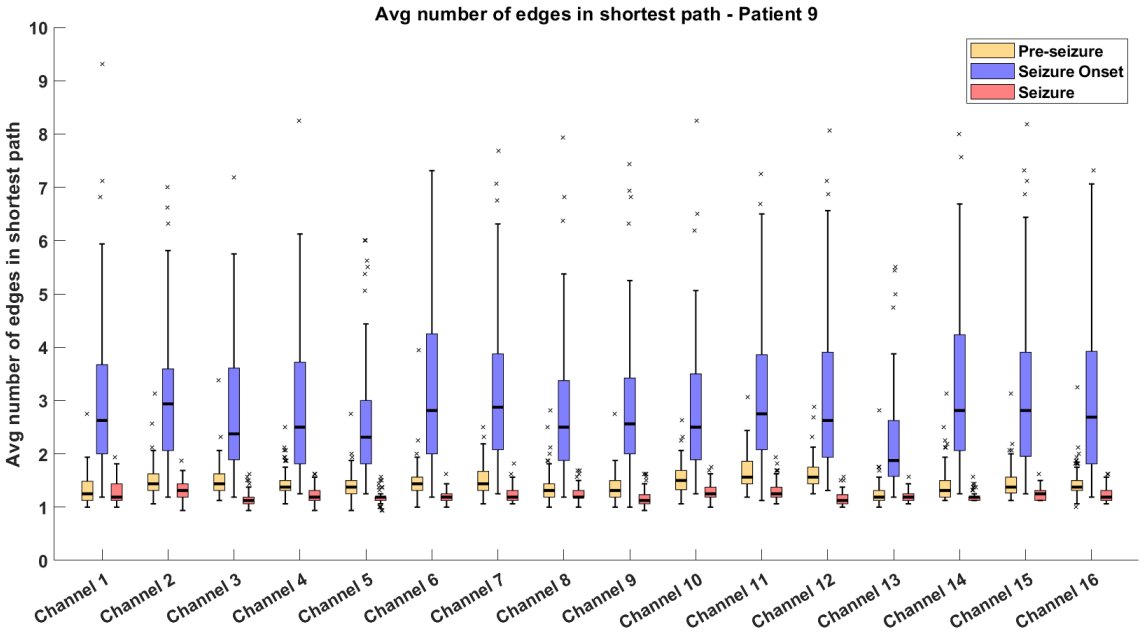

Figure 8. *The average number of edges in the shortest path for patient 9 across different seizure phases. The plot on the left shows the average during the pre-seizure phase, the middle plot represents the average at seizure onset, and the right plot illustrates the average during the seizure. The x-axis represents the 16 EEG channels.*

On the other hand, Figure 9 depicts the analysis of the clustering coefficient. In the pre-seizure phase, the clustering coefficients are generally low, mostly around 0.05, indicating sparse local interconnectedness among EEG channels. At seizure onset, a slight decrease in clustering coefficients is observed compared to pre-seizure. This decrease occurs in most of the channels. In the post-seizure phase, there is a marked increase in clustering coefficients, with many channels exhibiting values above 0.25. In absolute terms, the coefficient increase in the seizure is more evident than the decrease in the seizure onset. However, this reduced clustering coefficient suggests that local connections become weaker and less synchronized at seizure onset, which correlates with the findings of the shortest paths mentioned above.

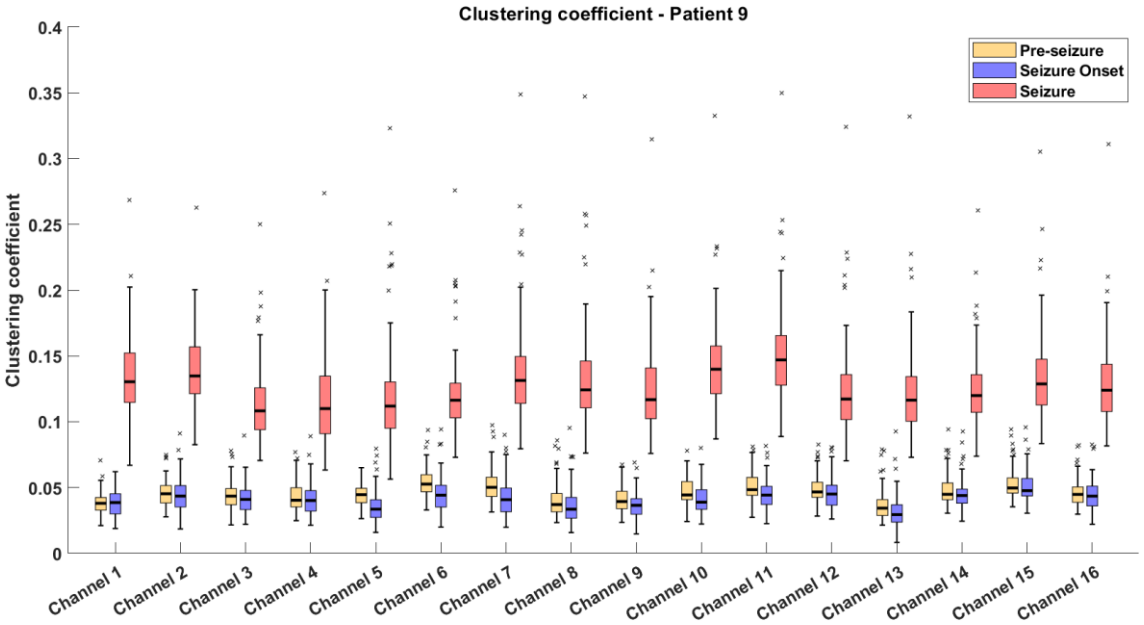

Figure 9. *The average clustering coefficient for each channel for patient 9 across different seizure phases. The plot on the left shows the average during the pre-seizure phase, the middle plot represents the average at seizure onset, and the right plot illustrates the average during the seizure. The x-axis represents the 16 EEG channels.*

Regarding the analysis of the betweenness centrality (Figure 10), in the pre-seizure phase, most channels exhibit low betweenness centrality, indicating a relatively stable network with minimal central nodes, except for channel 13, which shows higher centrality and variability. At seizure onset, there is a dramatic increase in betweenness centrality values across many channels, particularly channels 1, 3, 4, 5, 7, 8, 9, 10 and 13. This suggests a significant network reorganization where these channels become crucial for communication pathways, playing a key role in the propagation of seizure activity. During seizure, the network stabilizes with betweenness centrality values decreasing across all the channels, yielding values lower than pre-seizure levels.

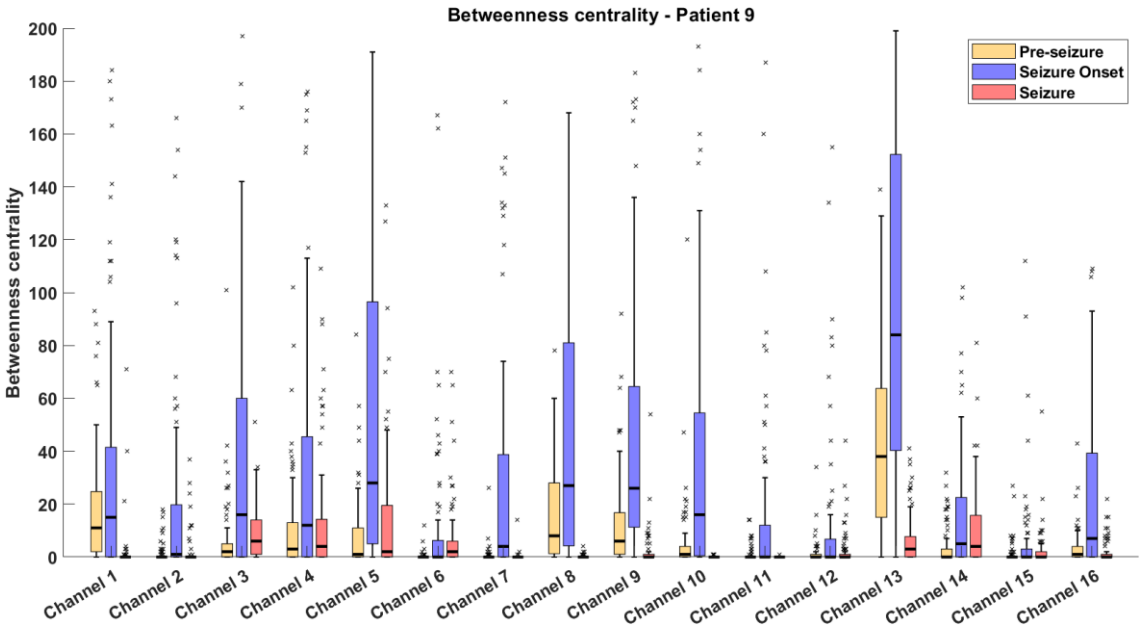

Figure 10. *The average channel betweenness centrality for patient 9 across different seizure phases. The plot on the left shows the average during the pre-seizure phase, the middle plot represents the average at seizure onset, and the right plot illustrates the average during the seizure. The x-axis represents the 16 EEG channels.*

Finally, the node strength findings reveal similar patterns found for the clustering coefficient (Figure 11). During the seizure onset, node strength stays around 1, indicating a baseline level of connectivity among brain regions. At the onset, most channels have a similar node strength distribution compared to the pre-seizure period. Here, what is interesting is that channel 13 has the lowest strength among all the channels, which is also the channel with the highest betweenness centrality at this stage. Then, as the seizure unfolds, node strength escalates to approximately 5, signifying a significant increase in connectivity. The heightened node strength during seizure reflects intensified interactions among key regions, potentially facilitating synchronized neural activity characteristic of seizure events. In the case of this patient, channel 15 has the highest node strength during seizure onset, suggesting it might be a central hub. These hubs play pivotal roles in coordinating network communication and are crucial for maintaining functional organization in the brain.

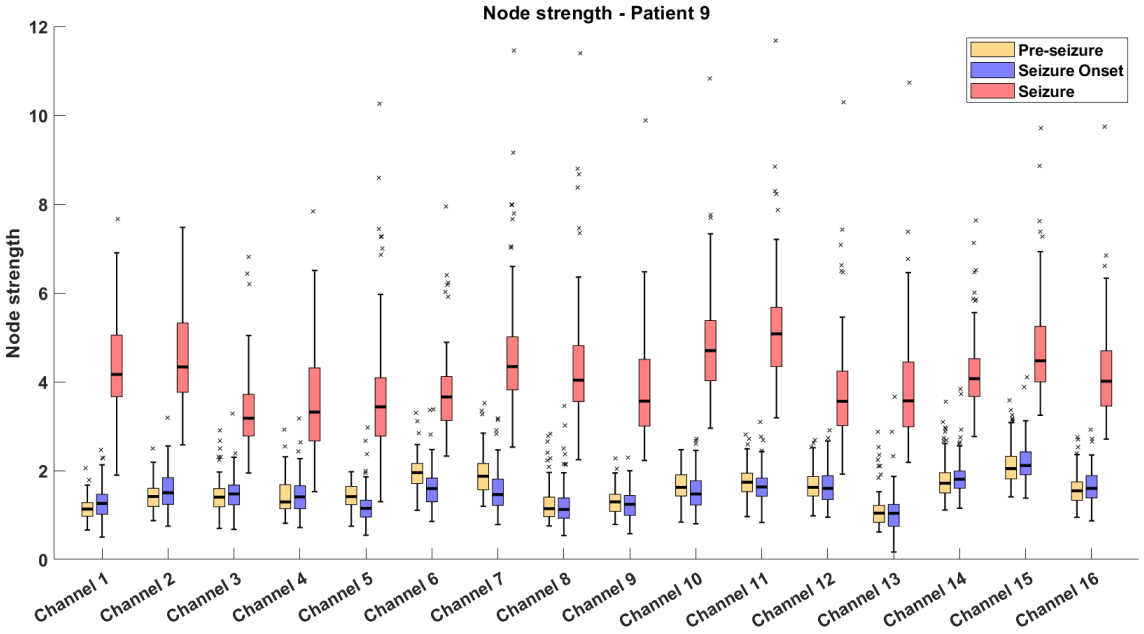

Figure 11. *The average channel strength for patient 9 across different seizure phases. The plot on the left shows the average during the pre-seizure phase, the middle plot represents the average at seizure onset, and the right plot illustrates the average during the seizure. The x-axis represents the 16 EEG channels.*

3.3.2. Patient-wise network comparison

The analysis of the average shortest paths across three periods (pre-seizure, seizure onset, and seizure) for the ten patients reveals distinct connectivity patterns (Figure 12). For most patients, there is a significant increase in the average shortest path at seizure onset compared to the pre-seizure period. This increase is highly significant ($p < 0.001$) for Patients 1, 3, 6, 7, 8, 9, 10, and 13. Patient 9 exhibits the largest shortest paths during seizure onset, followed by Patients 6 and 8, indicating a heightened level of network complexity and potential reorganization as the seizure begins. On the other hand, despite

the increase from the pre-seizure stage, Patients 1, 11, and 13 have relatively short shortest paths, consistent with their overall lower average connectivity values shown in Figure 5.

During the seizure period, the average shortest path generally decreases from the seizure onset phase. This decrease is statistically significant ($p < 0.001$) for all patients except for Patient 11. During the seizure, the median shortest path includes between 1 and 2 nodes for all patients, but Patients 6, 9, and 15 show the lowest numbers. These patients also have the highest average seizure lengths of all patients (refer to Table 2) and on average, higher mean connectivity (Figure 5) compared to the rest of the patients. This suggests that prolonged seizure activity may be associated with reduced network complexity and fewer connections in the shortest paths.

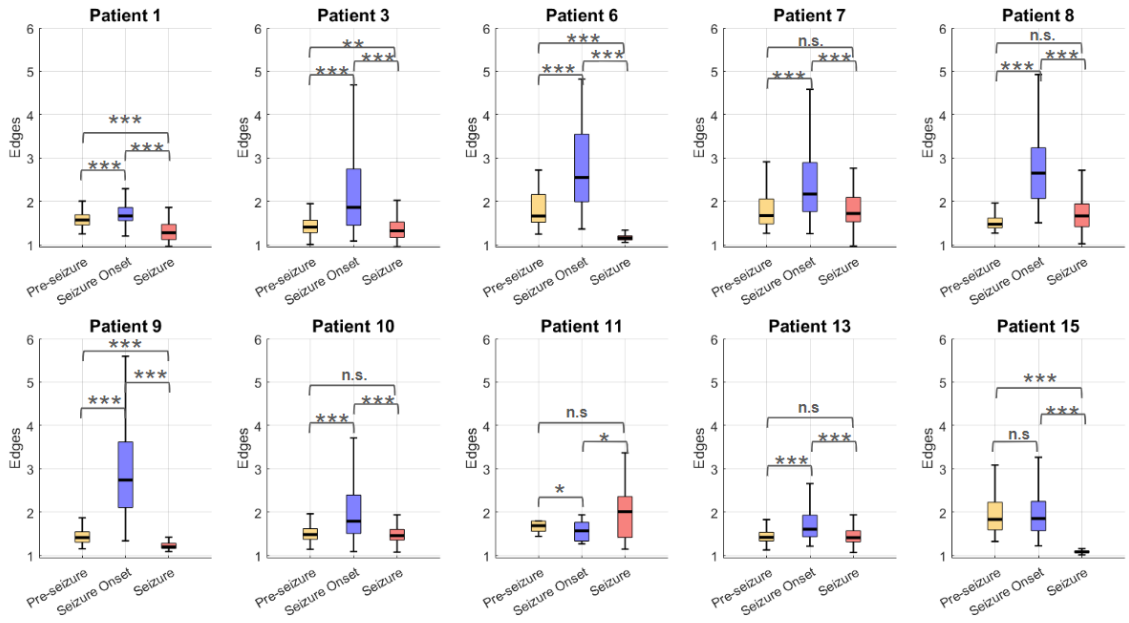

Figure 12. *Average number of edges in the shortest path across all 16 EEG channels for three periods (pre-seizure, seizure onset, seizure) in ten patients. Significance between each period pair is indicated for each patient. Significance levels: *** $p < 0.001$, ** $p < 0.01$, * $p < 0.05$, n.s. = not significant.*

The clustering coefficient analysis (Figure 13) reveals a significant increase from the pre-seizure to seizure onset period for most patients. During the pre-seizure period, clustering coefficients are relatively low (0.05 to 0.1), indicating a less clustered network structure. At seizure onset, there is a noticeable rise in clustering coefficients, suggesting a transition to a more clustered network. This trend continues into the seizure period, where the coefficients often peak, reflecting a highly clustered network structure.

Notably, Patients 1, 6, 9, and 15 exhibit significantly higher clustering coefficients during seizures. As mentioned earlier, these are the patients with the highest average connectivity values, with Patient 15 showing the highest clustering, correlating with its previously noted highest average connectivity values. This indicates that higher connectivity is associated with increased clustering, suggesting that these patients' neural networks become more tightly interconnected during seizures. Such high clustering could imply a

localized synchronization of neural activity, potentially contributing to the maintenance and spread of seizure activity.

On the other hand, Patients 7, 10, and 11 show more subtle changes in their clustering coefficients. Their networks do not transition to the same extent as those of Patients 1, 6, 9, and 15, indicating variability in how different patients' neural networks react during seizures.

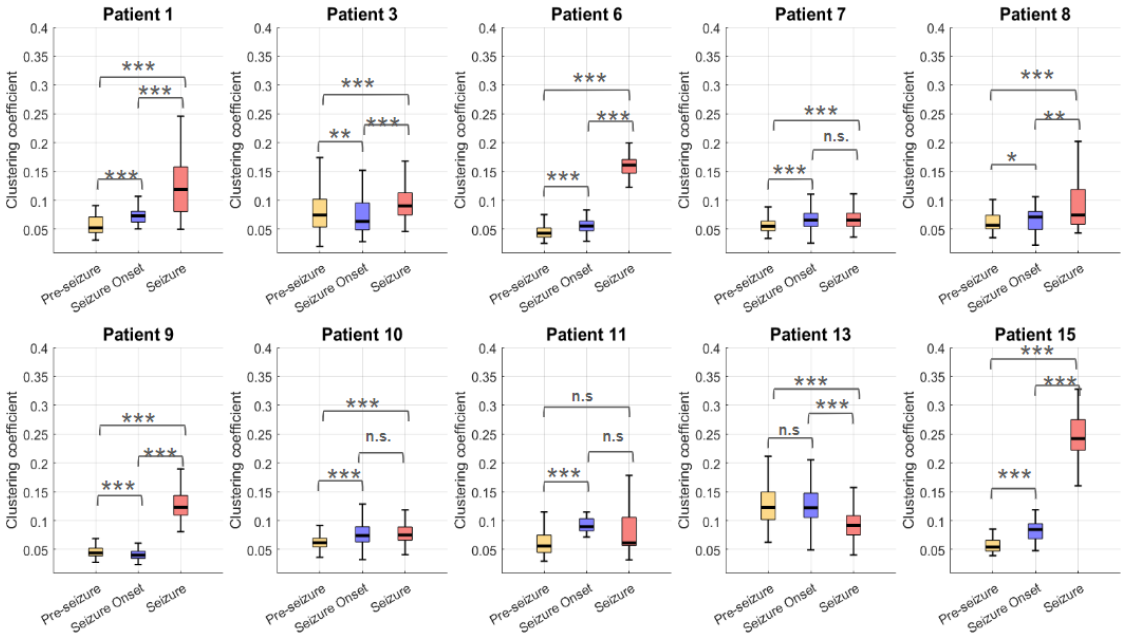

Figure 13. *Average clustering coefficient across all 16 EEG channels for three periods (pre-seizure, seizure onset, seizure) in ten patients. Significance between each period pair is indicated for each patient. Significance levels: *** $p < 0.001$, ** $p < 0.01$, * $p < 0.05$, n.s. = not significant.*

Regarding the betweenness centrality analysis (Figure 14), the data reveals that during the pre-seizure period, betweenness centrality values are generally low across all patients, indicating a less centralized network structure. At seizure onset, there is a marked increase in betweenness centrality for most patients, particularly for Patients 3, 6, 7, 8, and 9, with values reaching up to 60 ($p < 0.001$). This suggests a shift to a more centralized network where certain nodes become critical in maintaining connectivity. Notably, Patients 6 and 9, who exhibit higher mean connectivity, and Patients 3, 7, and 8, with lower mean connectivity, all show increased betweenness centrality, indicating that this measure does not directly correlate with seizure size or overall connectivity.

During the seizure period, the trend in average betweenness centrality becomes more varied but generally decreases drastically compared to seizure onset levels, with the exception of Patient 11, who appears to be an outlier. Patients 1, 6, 9, and 15 exhibit the lowest average betweenness centrality among all patients during seizures, significantly lower than their pre-seizure levels ($p < 0.001$). In contrast, Patient 8 shows a significant increase in average betweenness centrality during the seizure period ($p < 0.05$), while the rest of the patients do not experience significant differences compared to pre-seizure levels.

These findings suggest that average betweenness centrality is influenced by the mean connectivity of the network. Patients with higher mean connectivity tend to have lower betweenness centrality values, while those with lower mean connectivity exhibit higher betweenness centrality values during seizures. This indicates that betweenness centrality can provide unique insights into the network dynamics and the role of specific nodes during epileptic events.

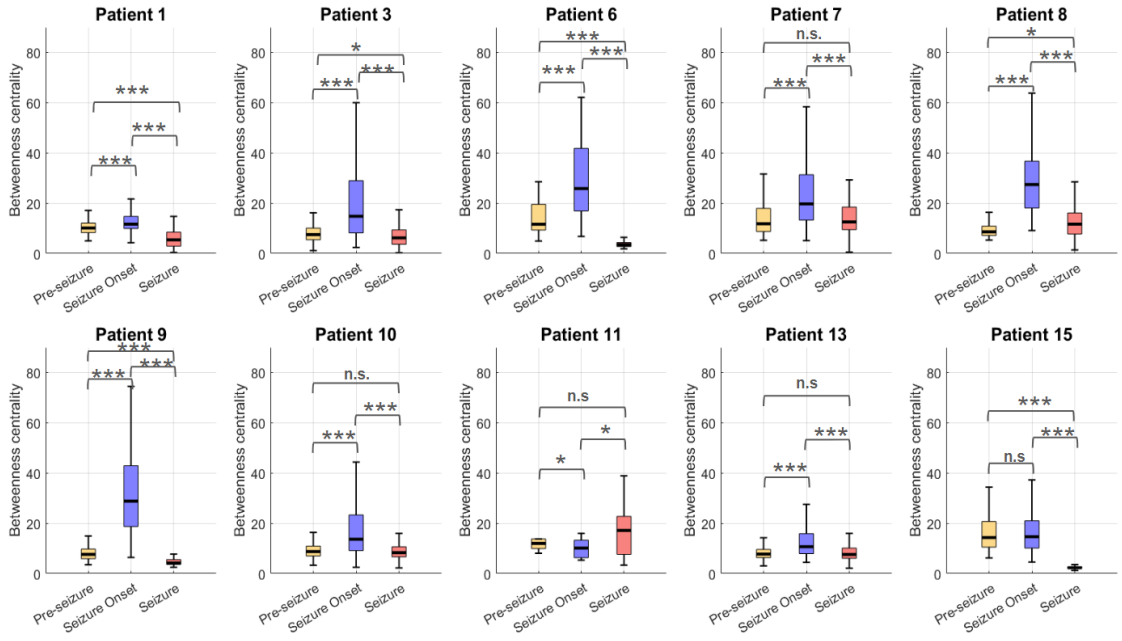

Figure 14. *Average betweenness centrality across all 16 EEG channels for three periods (pre-seizure, seizure onset, seizure) in ten patients. Significance between each period pair is indicated for each patient. Significance levels: *** p < 0.001, ** p < 0.01, * p < 0.05, n.s. = not significant.*

Finally, the results for average node strength also show a significant increase from the pre-seizure period to seizure onset, which continues to rise during the seizure phase. At seizure onset, the distribution of average strength is slightly higher than in the pre-seizure period; however, no distinctive patterns emerge between patients with higher connectivity and those with lower connectivity. This indicates that node strength at seizure onset may not be a reliable predictor of seizure magnitude. During the seizure phase, Patients 1, 6, 9, and 11 consistently exhibit the highest node strength values, mirroring the findings for clustering coefficients. This suggests heightened neural activity and stronger individual node activations in these patients during seizure events. Conversely, Patient 13 deviates from the general trend, showing a decrease in node strength during seizures, highlighting individual variability in neural network responses.

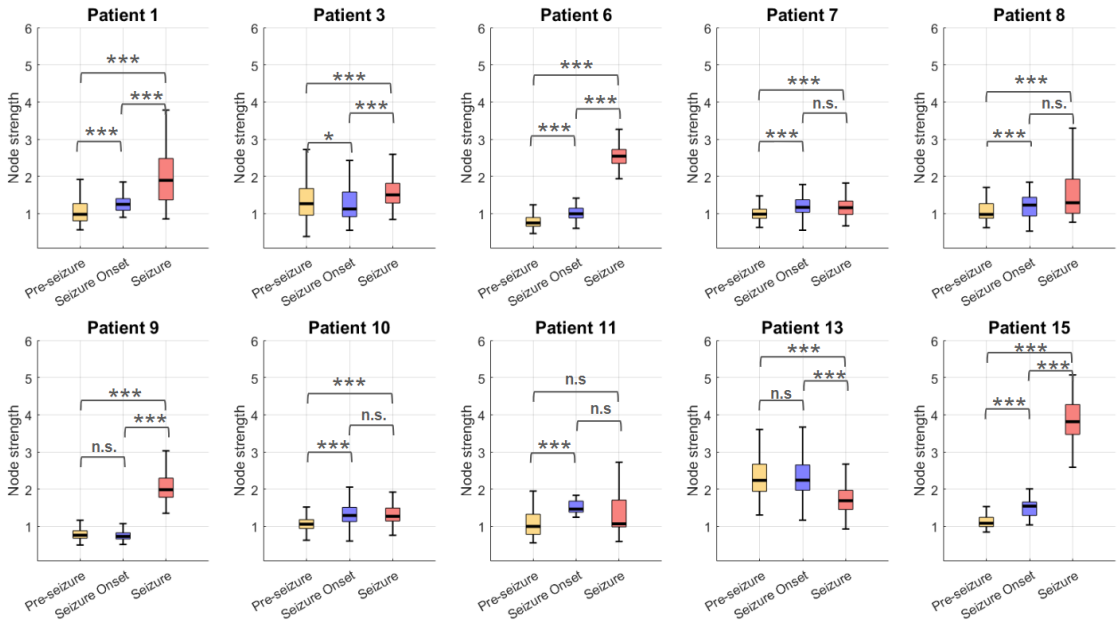

Figure 15. *Average channel strength across all 16 EEG channels for three periods (pre-seizure, seizure onset, seizure) in ten patients. Significance between each period pair is indicated for each patient. Significance levels: *** $p < 0.001$, ** $p < 0.01$, * $p < 0.05$, n.s. = not significant.*

3.4. Channel Influence

Finally, the method described earlier to account for the channel influence evolution over the duration of the seizure recording was tested. This approach aims to detect channels that exhibit significant connectivity alterations early in seizures, critical for SOZ identification.

In Figure 16 the net channel influence over time for patient 6 can be observed. During the pre-seizure period, all channels exhibit relatively stable influence with minimal fluctuations before the seizure onset. Then, at the seizure onset, channels such as channel 4, channel 7, channel 12 or channel 14 exhibit a marked increase in influence at seizure onset. This suggests these channels are actively involved in the initiation and early propagation of seizure activity. On the other hand, channels like channel 5, channel 6 and channel 9 show a negative net channel influence, indicating that these channels are receiving more information than they are giving. In the post-seizure onset phase, the figure depicts high variability across all channels as indicated by the wide shaded error bars. This suggests significant variations in how the channels are involved in seizure activity across different seizures. In this period, channels like channel 2 and channel 3 notoriously exhibit low channel influence levels in comparison to the rest. Contrarily, channels 6, 12, 14 and 15 maintain high influence levels throughout the seizure period, implying their critical role in sustaining seizure dynamics.

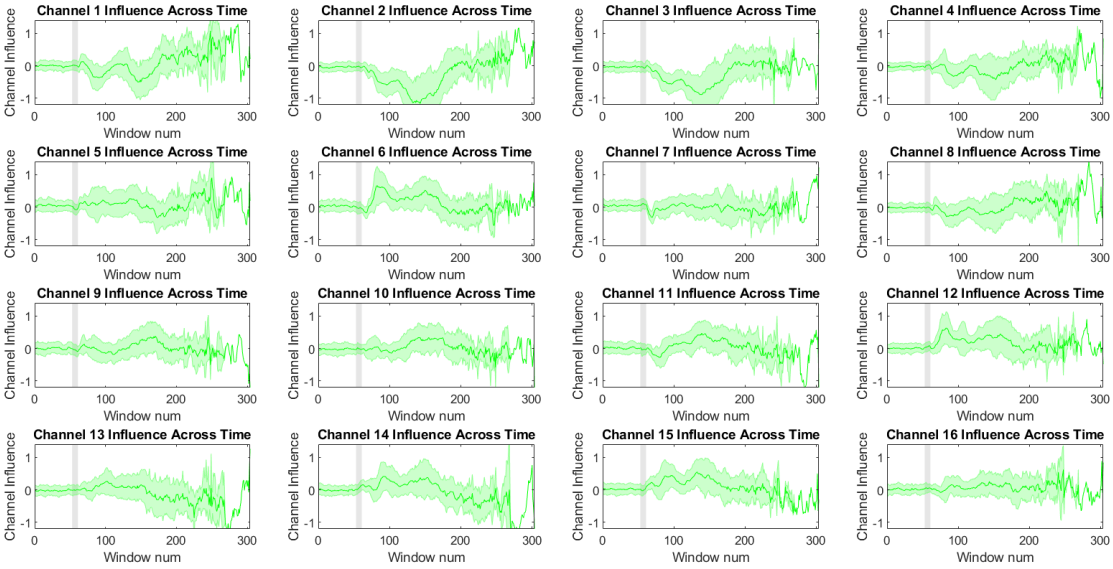

Figure 16. *Channel influence evolution across seizures in patient 6. The shaded grey area represents the seizure onset. Each subplot represents the influence of a specific channel across multiple time windows and seizures, with the solid green line indicating the mean influence and the shaded area representing the standard deviation.*

Regarding other patients, Figure 17 depicts the evolution of influence for patient 15. Similar to patient 6, this individual shows consistent influence levels across all channels during the pre-seizure stage. However, at seizure onset and throughout the seizure, intriguing patterns emerge. Specifically, electrode channels within the same stripe exhibit comparable behaviours.

For instance, at seizure onset, channels 1, 2, and 3 from the same stripe demonstrate a slight increase in influence, whereas channels 5, 6, and 7 show a decrease. Channels 13 and 16 also exhibit a minor decrease in influence. The packed behaviour becomes more pronounced following seizure onset. Channels 1, 2, and 3 initially show a stable influence pattern, which then increases slightly over time. In contrast, channels 5 and 6 display a declining trend early on. Channels 7 and 8 begin to gain influence shortly after seizure onset, reaching their peak around time window 100. Channels 9, 10, 11, and 12, belonging to the next stripe, start to increase in influence later, notably around time window 100. Finally, channels 13 to 16 in the fourth stripe maintain relatively stable influence across seizures, except for channel 16, which experiences a noticeable increase in influence. These observations underscore the complex dynamics of neural connectivity during seizures, highlighting distinct patterns within and across electrode stripes that may aid in understanding seizure onset and propagation in this patient cohort.

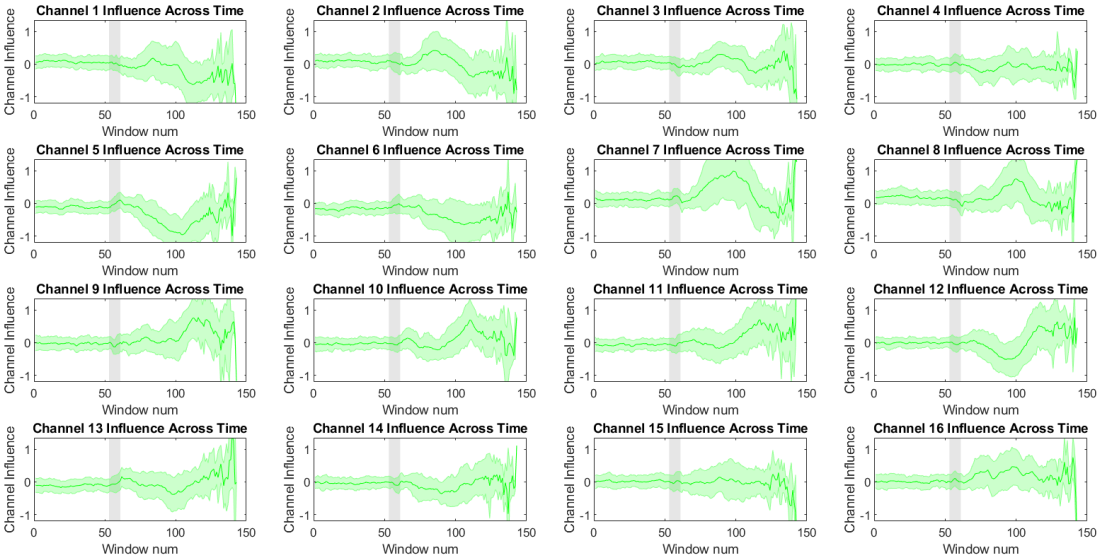

Figure 17. *Channel influence evolution across seizures in patient 15. The shaded grey area represents the seizure onset. Each subplot represents the influence of a specific channel across multiple time windows and seizures, with the solid green line indicating the mean influence and the shaded area representing the standard deviation.*

4. DISCUSSION

This study presents a comprehensive analysis of seizure data from ten drug-resistant focal epilepsy patients, highlighting the significant variability in seizure characteristics and connectivity patterns. The results underscore the complexity of epilepsy, demonstrating that seizure duration and intensity can vary widely among patients. For instance, it was observed that the only patient who was not under AED treatment, Patient 6, had the longest seizures. Notably, this analysis is based on EEGs recorded in natural environments rather than clinical settings, providing a more realistic representation of patients' seizure experiences.

The L measure applied to EEG data effectively captured differences in seizure intensity and connectivity. The comparison between a mild seizure from Patient 7 and a more intense seizure from Patient 6 demonstrated how the L matrices reflected the underlying neural activity. Mild seizures showed low connectivity, while intense seizures exhibited higher and more complex connectivity patterns. This reinforces the potential of the L measure as a tool for quantifying seizure dynamics.

On top of that, the network analysis of epileptic seizure dynamics used metrics like the shortest path, clustering coefficient, betweenness centrality, and node strength, offering insights from EEG data on individual patients and a comparison across a cohort of ten patients.

For Patient 9, we observed notable changes throughout the seizure progression. Initially, network centralization was moderate, with path lengths increasing at seizure onset, indicating decentralization. During seizures, path lengths decreased, showing a centralized network with increased direct connectivity, crucial for synchronized neural activity. Clustering coefficient analysis revealed a shift from sparse local connections pre-seizure to increased clustering and synchronization during seizures, suggesting tightly knit sub-networks that maintain and spread seizure activity. Betweenness centrality highlighted key nodes in network communication during seizures. Patient 9 showed a dramatic increase at seizure onset. Channel 13 had the highest centrality, indicating it could be in the SOZ. Node strength analysis corroborates these findings, with increased node strength during seizure onset, indicating intensified interactions among key brain regions. This increase was particularly high for Channel 15. Hence, the metric results for Patient 9 suggest that Channels 13 and 15, likely part of the same electrode strip, can be identified as potential central hubs, suggesting the SOZ is localized around these electrodes.

On the other hand, comparing network metrics across ten patients revealed variability and commonalities in network responses to seizure activity. Most patients showed significant increases in the shortest paths at seizure onset, highlighting enhanced network complexity early in seizures. During seizures, there was a trend towards more centralized network configurations. In addition, it was seen that patients with longer and higher connectivity seizures had the shortest paths during seizures, suggesting these networks have lower complexities to transmit information. Clustering coefficients increased significantly from pre-seizure to seizure onset for most patients, with those having higher mean connectivity showing pronounced increases during seizures. Betweenness centrality and node strength

analyses also reflected these patterns, underscoring the complex interplay between network structure, connectivity, and seizure dynamics across patients.

The most relevant finding, based on both the individual and inter-patient analyses, is the potential of shortest path and betweenness centrality for SOZ identification. These metrics displayed the most significant changes at seizure onset compared to pre-seizure and seizure stages, suggesting their crucial role in characterizing seizure initiation. During seizure onset, the brain network undergoes significant changes. The metrics like shortest path and betweenness centrality capture this disruption. These metrics become more sensitive at seizure onset because they reflect the initial breakdown in normal communication patterns within the brain network. This insight paves the way for future SOZ identification strategies that focus more heavily on these network graph metrics.

Finally, the study's analysis of channel influence revealed important insights that complement the findings from the graph theory analysis. At seizure onset, certain channels showed increased influence, suggesting their role in initiating epileptic activity. At the same time, other channels had negative net influence, indicating they primarily received propagated seizure signals from the channels that had a net positive influence. In addition to that, the time evolution pattern of the channel influence also highlights the dynamic nature of seizures. Some channels consistently showed lower influence, suggesting limited involvement in sustaining seizure activity. Others maintained high influence, indicating a crucial role in sustaining and propagating seizures. Besides, Patient 15 exhibited similar influence patterns across electrodes within the same stripe, suggesting that spatial proximity and electrode placement significantly affect channel behaviour during seizures. These findings align with previous research by Grau et al. [18] highlighting that connectivity changes can help in SOZ identification.

While the study offers valuable insights, a key limitation lies in the lack of precise information regarding the spatial location of the 16 EEG electrodes. The NeuroVista trial suggests placement in four-electrode strips on the focal zone, which varies for each patient. However, the exact proximity of each electrode to the SOZ remains unknown. This limitation highlights the need for future studies to incorporate electrode localization labels to further strengthen the generalizability and clinical applicability of the findings.

5. CONCLUSION

In conclusion, this study sheds light on the complexities of epilepsy by analyzing seizure data from drug-resistant patients in natural environments. The findings highlight significant variability in seizure characteristics and connectivity patterns across individuals. Notably, the use of the L measure and network analysis metrics like shortest path, clustering coefficient, betweenness centrality, and node strength provided valuable insights into seizure dynamics.

One of the most significant outcomes is the potential of shortest path and betweenness centrality for SOZ identification. These metrics displayed the greatest changes at seizure onset, pinpointing the crucial role of this stage in characterizing seizure initiation. This finding paves the way for future SOZ identification strategies that focus more on network analysis of seizure onset.

Furthermore, the analysis of channel influence offered complementary insights, revealing specific channels with increased influence at seizure onset, suggesting their role in initiating epileptic activity. These findings, along with the observed network dynamics, enhance our understanding of the underlying mechanisms of seizure initiation and propagation.

Despite the valuable insights gained, a key limitation of the study was the lack of precise information regarding electrode locations. Future research incorporating actual electrode localization can strengthen the generalizability and clinical applicability of these findings. Future studies should also leverage these network metrics findings for the automatic detection of the SOZ, by means of an unsupervised machine learning algorithm. Additionally, longitudinal studies involving larger patient cohorts are also necessary to validate these findings across diverse seizure types and patient demographics. This could provide more comprehensive insights into seizure mechanisms and support the development of personalized treatment strategies for epilepsy patients.

BIBLIOGRAPHY

[1] Epilepsy Foundation. What is epilepsy? Available from: https://www.epilepsy.com/what-is-epilepsy

[2] Epilepsy Foundation. Understanding Seizures. Available from: https://www.epilepsy.com/what-is-epilepsy/understanding-seizures

[3] Duncan JS, Sander JW, Sisodiya SM, Walker MC. (2006) Adult epilepsy. Lancet 367: 1087–1100.

[4] Kwan P, et al. Epilepsia. 2009;50(5):1043-57. DOI: 10.1111/j.1528-1167.2009.02397.x

[5] Luoni C, Bisulli F, Canevini MP, De Sarro G, Fattore C, Galimberti CA, Gatti G, La Neve A, Muscas G, Specchio LM, Striano S, Perucca E. (2011) Determinants of health-related quality of life in pharmacoresistant epilepsy: results from a large multicenter study of consecutively enrolled patients using validated quantitative assessments. Epilepsia 52: 2181–2191.

[6] Jayakar, P., Gotman, J., Harvey, A. S., Palmini, A., Tassi, L., Schomer, D., Dubeau, F., Bartolomei, F., Yu, A., Kršek, P., Velis, D., & Kahane, P. (2016). Diagnostic utility of invasive EEG for epilepsy surgery: Indications, modalities, and techniques. Epilepsia, 57(11), 1735–1747. https://doi.org/10.1111/epi.13515

[7] Rosenow, F., & Lüders, H. (2001). Presurgical evaluation of epilepsy. Brain : a journal of neurology, 124(Pt 9), 1683–1700. https://doi.org/10.1093/brain/124.9.1683

[8] Staljanssens, W., Strobbe, G., Holen, R. V., Birot, G., Gschwind, M., Seeck, M., Vandenberghe, S., Vulliémoz, S., & van Mierlo, P. (2017). Seizure Onset Zone Localization from Ictal High-Density EEG in Refractory Focal Epilepsy. Brain topography, 30(2), 257–271. https://doi.org/10.1007/s10548-016-0537-8

[9] Krucoff, M. O., Chan, A. Y., Harward, S. C., Rahimpour, S., Rolston, J. D., Muh, C., Englot, D. J. (2017). Rates and predictors of success and failure in repeat epilepsy surgery: A meta-analysis and systematic review. Epilepsia, 58(12), 2133–2142. https://doi.org/10.1111/epi.13920

[10] Quitadamo, L. R., Mai, R., Gozzo, F., Pelliccia, V., Cardinale, F., Seri, S. (2018). Kurtosis-based detection of intracranial high-frequency oscillations for the identification of the seizure onset zone. International journal of neural systems, 28(07), 1850001.

[11] Panzica, F., Varotto, G., Rotondi, F., Spreafico, R., Franceschetti, S. (2013). Identification of the Epileptogenic Zone from Stereo-EEG Signals: A Connectivity-Graph Theory Approach. Frontiers in neurology, 4, 175. https://doi.org/10.3389/fneur.2013.00175

[12] Varotto, G., Tassi, L., Franceschetti, S., Spreafico, R., & Panzica, F. (2012). Epileptogenic networks of type II focal cortical dysplasia: a stereo-EEG study. NeuroImage, 61(3), 591–598. https://doi.org/10.1016/j.neuroimage.2012.03.090

[13] Dauwels, J., Eskandar, E., & Cash, S. (2009). Localization of seizure onset area from intracranial non-seizure EEG by exploiting locally enhanced synchrony. Annual International Conference of the IEEE Engineering in Medicine and Biology Society. IEEE Engineering in Medicine and Biology Society. Annual International Conference, 2009, 2180–2183. https://doi.org/10.1109/IEMBS.2009.5332447

[14] Sharma, A., Rai, J. K., & Tewari, R. P. (2015). Epileptic seizure prediction and identification of epileptogenic region using EEG signal. In *2015 International Conference on Green Computing and Internet of Things (ICGCIoT)* (pp. 1194-1198). IEEE.

[15] Nuwer M. R. (1988). Frequency analysis and topographic mapping of EEG and evoked potentials in epilepsy. *Electroencephalography and clinical neurophysiology*, *69*(2), 118–126. https://doi.org/10.1016/0013-4694(88)90207-6

[16] Sharma, A., Rai, J. K., & Tewari, R. P. (2016). Anticipation of epileptic seizure in advance and localization of seizure onset zone using power spectral density. In *2016 Second International Innovative Applications of Computational Intelligence on Power, Energy and Controls with their Impact on Humanity (CIPECH)* (pp. 159-164). IEEE.

[17] Chicharro, D., & Andrzejak, R. G. (2009). Reliable detection of directional couplings using rank statistics. Physical Review E, 80(2), 026217.

[18] Leguia, M. G., Martínez, C. G., Malvestio, I., Campo, A. T., Rocamora, R., Levnajić, Z., & Andrzejak, R. G. (2019). Inferring directed networks using a rank-based connectivity measure. Physical Review E, 99(1), 012319.

[19] Moreno, V. (2023) Uncovering seizure connectivity and directionality patterns across patients with focal epilepsy. http://hdl.handle.net/10230/57961

[20] Cook, M. J., O'Brien, T. J., Berkovic, S. F., Murphy, M., Morokoff, A., Fabinyi, G., D'Souza, W., Yerra, R., Archer, J., Litewka, L., Hosking, S., Lightfoot, P., Ruedebusch, V., Sheffield, W. D., Snyder, D., Leyde, K., & Himes, D. (2013). Prediction of seizure likelihood with a long-term, implanted seizure advisory system in patients with drug-resistant epilepsy: a first-in-man study. The Lancet. Neurology, 12(6), 563–571. https://doi.org/10.1016/S1474-4422(13)70075-9

[21] Epilepsy Ecosystem. (n.d.). NeuroVista trial data. Retrieved from https://www.epilepsyecosystem.org/neurovista-trial-1#data

[22] The MathWorks Inc. (2022). MATLAB version: 9.10.0 (R2021a), Natick, Massachusetts: The MathWorks Inc. https://www.mathworks.com

[23] Rubinov, M., Sporns, O. (2010). Complex network measures of brain connectivity: uses and interpretations. *NeuroImage*, *52*(3), 1059–1069. https://doi.org/10.1016/j.neuroimage.2009.10.003

[24] Bullmore, E., Sporns, O. (2009). Complex brain networks: graph theoretical analysis of structural and functional systems. *Nature reviews. Neuroscience*, *10*(3), 186–198. https://doi.org/10.1038/nrn2575

[25] Mehraram, R., Kaiser, M., Cromarty, R., Graziadio, S., O'Brien, J. T., Killen, A., Peraza, L. R. (2020). Weighted network measures reveal differences between dementia types: An EEG study. *Human brain mapping*, *41*(6), 1573-1590.

[26] Rubinov, M., Kötter, R., Hagmann, P., Sporns, O. (2009). Brain connectivity toolbox: A collection of complex network measurements and brain connectivity datasets. *NeuroImage*, *47*(Supplement 1), S169. https://doi.org/10.1016/S1053-8119(09)71822-1

[27] Deo, N. (2016). *Graph theory with applications to engineering and computer science*. Courier Dover Publications.

[28] Dijkstra, E. W. (1959). A note on two problems in connexion with graphs. Numerische Mathematik, 1(1), 269-271.

[29] Cormen, T. H., Leiserson, C. E., Rivest, R. L., & Stein, C. (2009). *Introduction to algorithms*. MIT Press.

[30] Zemanová, L., Zhou, C., Kurths, J. (2006). Structural and functional clusters of complex brain networks. *Physica D: Nonlinear Phenomena*, *224*(1-2), 202-212.

[31] Brandes, U. (2001). A faster algorithm for betweenness centrality. *Journal of mathematical sociology*, *25*(2), 163-177.

[32] Kintali, S. (2008). Betweenness centrality: Algorithms and lower bounds. *arXiv preprint arXiv:0809.1906*.

[33] Geier, C., Bialonski, S., Elger, C. E., & Lehnertz, K. (2015). How important is the seizure onset zone for seizure dynamics?. *Seizure*, *25*, 160–166. https://doi.org/10.1016/j.seizure.2014.10.013

[34] Martínez, I. (2022). *Analysis of EEG signals for brain connectivity evaluation under emotional stimuli* (Bachelor's thesis, Universitat Politècnica de València). Retrieved from https://m.riunet.upv.es/bitstream/handle/10251/196865/Martinez%20-%20Analysis%20of%20EEG%20signals%20for%20brain%20connectivity%20evaluation%20under%20emotional%20stimuli.pdf?sequence=2&isAllowed=y

[35] Lilliefors, H. W. (1967). On the Kolmogorov-Smirnov test for normality with mean and variance unknown. *Journal of the American Statistical Association*, *62*(318), 399-402. https://doi.org/10.1080/01621459.1967.10482916

[36] Student. (1908). The probable error of a mean. *Biometrika*, *6*(1), 1-25. https://doi.org/10.2307/2331554

[37] Wilcoxon, F. (1945). Individual comparisons by ranking methods. *Biometrics Bulletin*, *1*(6), 80-83. https://doi.org/10.2307/3001968

SUPPORTING INFORMATION

SI-1. L measure applied to EEG.

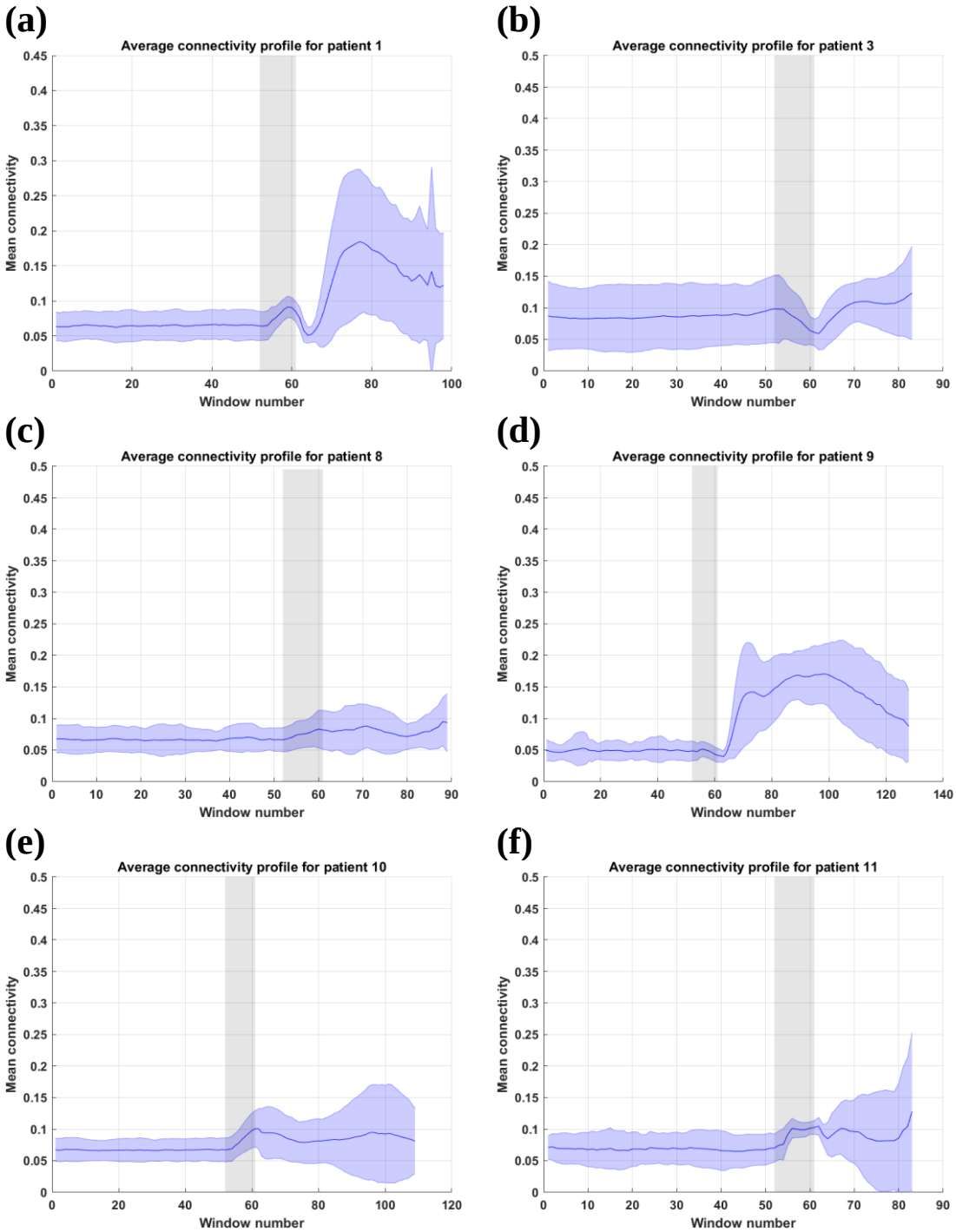

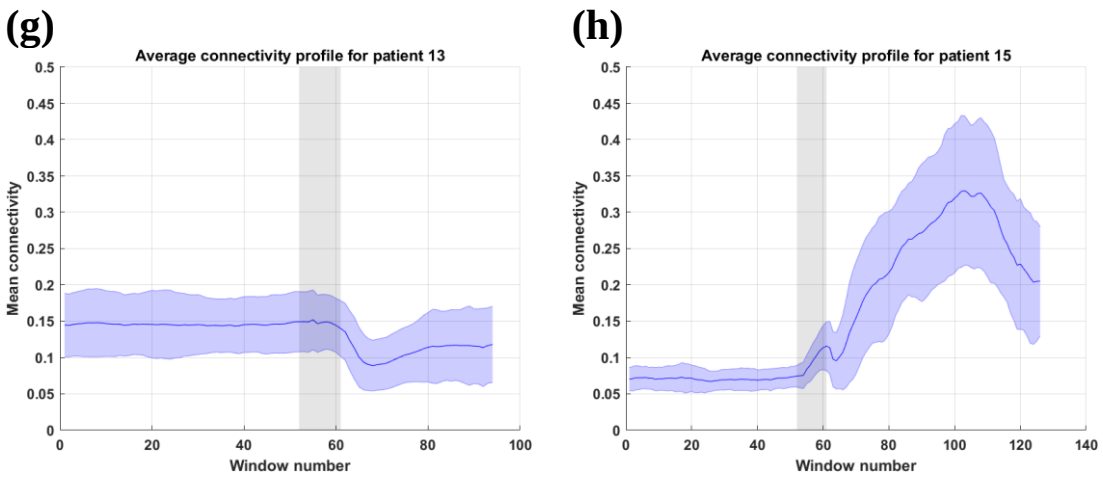

Figure SI-1. *The figure illustrates the connectivity profiles for seizures from (a) Patient 1; (b) Patient 3; (c) Patient 8; (d) Patient 9; (e)Patient 10; (f) Patient 11; (g) Patient 13; (h) Patient 15. Each panel displays the average connectivity profile across all seizures for a patient, with the shaded area representing the standard deviation. The x-axis denotes the window number, while the y-axis represents the mean connectivity.*